Summertime nitrate aerosol in the upper troposphere and lower stratosphere over the Tibetan Plateau and the South Asian summer monsoon region

Yixuan Gu[a,b], Hong Liao[a,*], and Jianchun Bian[c]

[a]State Key Laboratory of Atmospheric Boundary Layer Physics and Atmospheric Chemistry (LAPC), Institute of Atmospheric Physics, Chinese Academy of Sciences, Beijing, China.

[b]University of Chinese Academy of Sciences, Beijing, China

[c]Key Laboratory of Middle Atmosphere and Global Environment Observation (LAGEO), Institute of Atmospheric Physics, Chinese Academy of Sciences, Beijing, China.

*Corresponding author address:

Prof. Hong Liao

LAPC, Institute of Atmospheric Physics

Chinese Academy of Sciences

Beijing 100029, China

E-mail: hongliao@mail.iap.ac.cn

Abstract

We use the global three-dimensional Goddard Earth Observing System chemical transport model (GEOS-Chem) to examine the contribution of nitrate aerosol to aerosol concentrations in the upper troposphere and lower stratosphere (UTLS) over the Tibetan Plateau and the South Asian summer monsoon (TP/SASM) region during summertime of year 2005. Simulated surface-layer aerosol concentrations are compared with ground-based observations, and simulated aerosols in the UTLS are evaluated by using the Stratospheric Aerosol and Gas Experiment II satellite data. Simulations show elevated aerosol concentrations of sulfate, nitrate, ammonium, black carbon, organic carbon, and $PM_{2.5}$ (particles with diameter equal or less than 2.5 μm, the sum of sulfate, nitrate, ammonium, black carbon, and organic carbon aerosols) in the UTLS over the TP/SASM region throughout the summer. Nitrate aerosol is simulated to be of secondary importance near the surface but the most dominant aerosol species in the UTLS over the studied region. Averaged over summertime and over the TP/SASM region, C_{NIT} (the ratio of nitrate concentration to $PM_{2.5}$ concentration) values are 5–35% at the surface, 25–50% at 200 hPa, and could exceed 60% at 100 hPa. The mechanisms for the accumulation of nitrate in the UTLS over the TP/SASM region include vertical transport and the gas-to-aerosol conversion of HNO_3 to form nitrate. The high relative humidity and low temperature associated with the deep convection over the TP/SASM region are favorable for the gas-to-aerosol conversion of HNO_3.

1 Introduction

Aerosols in the upper troposphere and lower stratosphere (UTLS) have much longer residence times than those in the lower troposphere, influencing atmospheric chemistry and the Earth's climate with large spatial and temporal coverage (Rasch et al., 2008). Aerosols in the UTLS influence the concentrations of chemical species via changes in photolysis rates and heterogeneous reactions (Pitari et al., 2014). For example, heterogeneous reactions on sulfate aerosol can perturb the chemical partitioning in the lower stratosphere, leading to significant O_3 depletion through enhanced chlorine, bromine, and odd-hydrogen catalytic cycle (Zhao et al., 1997; Considine et al., 2001; Talukdar et al., 2012; Tang et al., 2014; Pitari et al., 2014). Aerosols in the UTLS also influence climate by altering properties of cirrus clouds via homogeneous or heterogeneous ice nucleation (Li et al., 2005; Liu et al., 2009; Yin et al., 2012; Fadnavis et al., 2013). Injection of aerosols into the UTLS has been reported to induce complex responses in circulation, temperature, and water vapor (Liu et al., 2009; Wu et al., 2011; Su et al., 2011; Fadnavis et al., 2013).

Aerosols over the Tibetan Plateau (TP) and the Asian summer monsoon region are especially important. The TP is surrounded by countries with large anthropogenic emissions (Li et al., 2005; Lau et al., 2006). Aerosols from India, Southeast Asia, and southern China can be transported to the TP by prevailing winds in the premonsoon and monsoon seasons (Lawrence and Lelieveld, 2010; Xia et al., 2011). Observational and modeling studies have shown that persistent maxima of atmospheric constituents, such as water vapor (Gettelman et al., 2004; Randel and Park, 2006; Park et al., 2007), CO (Kar et

al., 2004; Li et al., 2005; Park et al., 2007, 2008, 2009), CH_4 (M. Park et al., 2004; Xiong et al., 2009), NO_x (M. Park et al., 2004), HCN (Park et al., 2008; Randel et al., 2010), C_2H_6 and C_2H_2 (Park et al., 2008), exist in the UTLS above the TP and the South Asian summer monsoon (SASM) region because of the deep convection during boreal summer. Satellite observations suggested that the convection associated with the SASM is a vital pathway to transport air mass from the lower troposphere into the stratosphere (Chen et al., 2006; Randel and Park, 2006; Randel et al., 2010; Bian et al., 2011a). The heating associated with the persistent deep convection during summertime leads to the formation of the Tibetan anticyclone in the UTLS, which acts to isolate air within the anticyclone and traps the uplifted pollutants at that altitude (Park et al., 2007; Vernier et al., 2011; Bourgeois et al., 2012; Fadnavis et al., 2013; He et al., 2014). The stratosphere-troposphere exchange (STE) over the TP contributes largely to the global STE (Chen et al., 2006).

Previous studies have reported that aerosols exist in the UTLS over the TP/SASM region. Kim et al. (2003) carried out optical measurements with a ground-based lidar in Lhasa from August to October of 1999, and found an enhancement in aerosol concentration near the local tropopause with scattering ratio (SR, the ratio of aerosol plus molecular backscatter to molecular backscatter alone) of 1.1–1.2. Tobo et al. (2007) reported an enhancement of sub-micron aerosols (effective radius r = 0.15–0.6 μm) near the summertime tropopause (about 130 to 70 hPa), on the basis of in situ balloon measurements from an Optical Particle Counter at the same location in August of 1999. Vernier et al. (2009) examined satellite measurements from the Cloud-Aerosol Lidar with Orthogonal Polarization (CALIOP) onboard

Cloud-Aerosol Lidar and Infrared Pathfinder Satellite Observation (CALIPSO) and reported the presence of small depolarizing particles with high SR values (about 1.20 at 532 nm) at 16–17 km altitude over South Asia in July and August of 2007 and 2008. Bourgeois et al. (2012) found that an aerosol layer existed at 16–18 km altitude over the Asian continent and Indian Ocean (20°S–30°N, 5–105°E) on the basis of the CALIOP observations. Recently, He et al. (2014) examined the vertical profiles of aerosol extinction coefficients measured with a Micro Pulse Lidar at Naqu, a meteorological station located in the central part of the TP, and also showed a maximum in aerosol extinction coefficient (~2.10^{-3} km^{-1}) in the UTLS (18–19 km) during the summer of 2011.

A number of previous studies have attempted to understand the chemical composition of aerosols in the UTLS. Froyd et al. (2009) measured aerosol composition with the National Oceanic and Atmospheric Administration (NOAA) single-particle mass spectrometer aboard the National Aeronautics and Space Administration (NASA) WB-57 high altitude aircraft platform, and reported that particles in the tropical tropopause layer were rich in nitrogen. Vernier et al. (2011) suggested that aerosol layer at the tropopause of Asia could be sulfur and/or organics, considering that Asian pollutants consisted of black carbon, organic carbon, SO_2, and NO_x (Park et al., 2009; Randel et al., 2010). Weigel et al. (2011) analyzed the volatility of aerosols obtained from in situ airborne measurements and reported that about 75–90 % of the particles in the tropical tropopause layer were volatile, but this study did not give any detailed analyses of chemical composition of aerosols. Bourgeois et al. (2012) showed, by using the ECHAM5.5-HAM2 model, that sulfate, water, and OC contributed, respectively, 53%, 29%, and 11% to aerosol extinction in the vicinity of the

tropical tropopause layer. The ECHAM5.5-HAM2 model used by Bourgeois et al. (2012) simulated all major aerosol species in the atmosphere except for nitrate.

Few previous studies have examined nitrate aerosol in the UTLS, although nitrate is expected to be important for the following reasons. First, emissions of precursors of nitrate, such as NO_x and NH_3, are high over India, Southeast Asia, and China (Streets et al., 2003; Datta et al., 2012; Huang et al., 2012). Second, simulated nitrate concentrations are high over those regions (Liao and Seinfeld, 2005; Mu and Liao, 2014; Lou et al., 2014). Third, measured concentrations of nitrate are comparable to or larger than those of sulfate at rural and urban sites in the SASM region. Shrestha et al. (2000) carried out measurements of aerosols at Phortse, Nepal, during September 1996–November 1997, and showed that the average concentration of nitrate during the monsoon season (June-September) was 0.34 μg m^{-3}, higher than that of sulfate (0.17 μg m^{-3}). Decesari et al. (2010) reported, on the basis of measurements at the Nepal Climate Observatory-Pyramid from 2006 to 2008, that the concentrations of nitrate and sulfate were 0.37 μg m^{-3} and 0.50 μg m^{-3}, respectively, during the monsoon season. Chatterjee et al. (2010) measured aerosols at a high altitude station in northeastern Himalayas during January-December 2005. They found that the average concentrations of fine-mode nitrate and sulfate were 3.31±2.25 μg m^{-3} and 3.80±2.9 μg m^{-3}, respectively. At Lahore, an urban site in Pakistan, the observed daytime nitrate concentration of 21.8 μg m^{-3} was also higher than sulfate concentration of 12.6 μg m^{-3} (Lodhi et al., 2009), as the observations were averaged over November 2005 to March 2006. Fourth, the low temperatures in the UTLS would favor

149 nitrate formation (Seinfeld and Pandis, 2006). Therefore, it is of interest to take
150 nitrate aerosol into consideration when we examine aerosols in the UTLS.
151 In this work we simulate nitrate aerosol and its contribution to aerosol
152 concentrations in the UTLS over the TP (70–105°E, 25–40°N) and the SASM
153 region (70–105°E, 10–25°N) by using the global chemical transport model
154 GEOS-Chem driven by the assimilated meteorological fields. These regions of
155 interest are shown in Fig. 1. Simulated surface-layer aerosol concentrations
156 are compared with ground-based observations, and simulated aerosols in the
157 UTLS are evaluated by using the Stratospheric Aerosol and Gas Experiment
158 II (SAGE II) satellite data. Section 2 is a brief description of the GEOS-Chem
159 model and numerical experiment. Section 3 presents the simulation and
160 evaluation of distributions and concentrations of HNO_3 and O_3 to show model's
161 capability in simulating the NO_x-O_3-HNO_3 cycle over the studied regions.
162 Section 4 shows simulated aerosols and Section 5 presents the simulated
163 contribution of nitrate to aerosol concentrations in the UTLS over the TP and
164 the SASM region. Section 6 discusses the mechanisms for high concentrations
165 of nitrate in the UTLS. Section 7 discusses the impacts of uncertainties in
166 surface-layer aerosol concentrations on simulated nitrate in the UTLS.
167
168 **2 Model description and numerical experiment**
169 **2.1 GEOS-Chem model**
170 We simulate gas-phase species and aerosols using the global chemical
171 transport model GEOS-Chem (version 9-01-03,
172 http://acmg.seas.harvard.edu/geos/index.html) driven by the GEOS-5
173 assimilated meteorological fields from the Goddard Earth Observing System of

174 the NASA Global Modeling and Assimilation Office. The version of the model
175 used here has a horizontal resolution of 2° latitude by 2.5° longitude and 47
176 vertical layers extending from the surface to 0.01 hPa. Over the TP and the
177 SASM region, the model has about 34 layers in the troposphere and 12 layers
178 in the stratosphere.

179 The GEOS-Chem model has a fully coupled treatment of tropospheric
180 NO_x-CO-hydrocarbon-aerosol chemistry and aerosols including sulfate (SO_4^{2-}),
181 nitrate (NO_3^-), ammonium (NH_4^+), organic carbon (OC), black carbon (BC) (R. J.
182 Park et al., 2003; 2004; Pye et al., 2009), mineral dust (Fairlie et al., 2007), and
183 sea salt (Alexander et al., 2005; Jaeglé et al., 2011). The gas-aerosol
184 partitioning of nitric acid and ammonium is calculated using the ISORROPIA II
185 thermodynamic equilibrium module (Fountoukis and Nenes, 2007). The
186 two-way coupling between aerosols and gas phase chemistry provides
187 consistent chemical fields for aerosol simulation and aerosol mass for
188 heterogeneous processes and calculations of gas-phase photolysis rates.
189 Heterogeneous reactions include hydrolysis of N_2O_5 (Evans and Jacob, 2005),
190 irreversible absorption of NO_3 and NO_2 on wet aerosols (Jacob, 2000), and the
191 uptake of HO_2 by aerosols (Liao and Seinfeld, 2005; Thornton et al., 2008).

192 With respect to chemistry in the stratosphere, stratospheric O_3
193 concentrations are calculated using the linearized parameterization scheme
194 (McLinden et al., 2000). The monthly mean production rates and loss
195 frequencies of other stratospheric species (including long-lived species such
196 as CFCs and N_2O) use those from NASA Global Modeling Initiative (GMI)
197 Combo simulations (Duncan et al., 2007; Considine et al., 2008; Murray et al.,
198 2012).

199 Convective transport in GEOS-Chem mimics that in the parent GEOS
200 general circulation model (GCM) (Hack, 1994; Zhang and McFarlane, 1995),
201 which accounts for updraft, downdraft, and entrainment mass fluxes for deep
202 and shallow convection (Wu et al., 2007). The aerosol wet deposition scheme
203 in the GEOS-Chem follows that of Liu et al. (2001). For the scavenging of
204 aerosols, SO_4^{2-}, NO_3^-, NH_4^+, and hydrophilic OC and BC aerosols are assumed
205 to be fully soluble. Dry deposition follows the standard resistance-in-series
206 model of Wesely (1989).
207 Global emissions of aerosols and their precursors in the GEOS-Chem
208 follow R. J. Park et al. (2003, 2004), with anthropogenic emissions of NO_x, CO,
209 SO_2, and non-methane volatile organic compounds (NMVOC) in Asia
210 overwritten by David Streets' 2006 emission inventory
211 (http://mic.greenresource.cn/intex-b2006). Emissions of NH_3 in Asia are taken
212 from Streets et al. (2003). Since NH_3 emissions in China showed large
213 uncertainties in previous studies (Streets et al., 2003; Kim et al., 2006; Y.
214 Zhang et al., 2010; Huang et al., 2011, 2012), we use the most recent estimate
215 of NH_3 emissions in China by Huang et al. (2012), which is 9.8 Tg yr^{-1}, instead
216 of 13.5 Tg yr^{-1} from Streets et al. (2003). Table 1 summarizes the annual
217 emissions of NO_x, SO_2, NH_3, OC, and BC in Asia domain (60–155°E,
218 10–55°N).
219 Natural NO_x emissions from lightning are calculated using the scheme
220 described by Sauvage et al. (2007) and Murray et al. (2012), and those from
221 soil are simulated following Wang et al. (1998). Natural NH_3 emissions from
222 soil, vegetation, and the oceans are taken from the Global Emissions Inventory
223 Activity inventory (Bouwman et al., 1997). Biomass burning emissions are from

the monthly Global Fire Emissions Database (GFED v3) driven by satellite observations of fire activity (van der Werf et al., 2010). Biogenic VOC (volatile organic compounds) emissions are calculated from the Model of Emissions of Gases and Aerosols from Nature (Guenther et al., 2006).

The monthly variations of emissions of SO_2 and NO_x follow Wang et al. (2013) and those of BC and OC follow Lou et al. (2014). The monthly scaling factors for NH_3 emissions follow the global inventory compiled by Marcel Meinders and Lex Bouwman (Fisher et al., 2011). Monthly variations of emissions (anthropogenic plus natural emissions) of NO_x SO_2, NH_3, OC, and BC over Asia are displayed in Fig. 2. The emissions of NH_3 are the highest in June as a result of the agriculture practice and high temperatures (Wang et al., 2013).

2.2 Numerical experiment

To examine the contribution of nitrate to aerosol concentrations in the UTLS over the TP/SASM region, we simulate aerosol concentrations by using the emissions of and meteorological fields of year 2005. Year 2005 is chosen so that we can use the observational datasets for this year from SAGE II and MLS, as described in Sects. 3 and 4. Following Rasch et al. (2008), we perform a 10-year spin-up run to generate the initial conditions (to allow the stratospheric species to reach quasi-steady state conditions). We would consider that the tropospheric simulation can be representative of year 2005 but stratosphere simulation should represent a multi-year average, because the production rates and loss frequencies in the stratosphere are the averages over years of 2004–2010 (http://wiki.seas.harvard.edu/geos-chem/index.php/ Stratospheric_ chemistry).

3 Simulated concentrations of HNO_3 and O_3 and model evaluation

Nitrate aerosol forms when nitric acid (HNO_3) reacts with alkaline gases (for example, ammonia) in the atmosphere (Seinfeld and Pandis, 2006). HNO_3, as the important precursor of nitrate, is the major oxidation product of nitrogen oxides (NO_x = NO+NO_2) (Seinfeld and Pandis, 2006). To show the model's capability in simulating the NO_x-O_3-HNO_3 cycle over the studied regions, we present and evaluate the simulated HNO_3 and O_3 in this section.

Simulated mixing ratios of HNO_3 and O_3 in the UTLS are evaluated by using datasets from the limb viewing satellite instrument of Microwave Limb Sounder (MLS, version 3.3, level 2, ftp://acdisc.gsfc.nasa.gov/data/s4pa///Aura_MLS_Level2/). The MLS datasets provide valuable information on atmospheric compositions in the UTLS (Waters et al., 2006). For HNO_3, the MLS provides datasets for 215 to 1.5 hPa, with a vertical resolution of 3–4 km and a horizontal resolution of 400–500 km. Since further evaluations are needed for datasets at altitudes with pressures higher than 215 hPa (Livesey et al., 2011), we use only datasets for pressures lower than that. For O_3, the MLS provides datasets for 261 to 0.02 hPa, with a vertical resolution of 2.5–3 km and a horizontal resolution of 300–400 km in the UTLS (Santee et al., 2007; Livesey et al., 2011). The uncertainties of the MLS HNO_3 and O_3 datasets in the UTLS are about ±0.5–1 ppbv (± 5–10%) and 0.02–0.04 ppmv, respectively (Livesey et al., 2011).

3.1 HNO_3

Figure 3(a) shows the simulated global distribution of HNO_3 concentrations averaged over June-August of 2005. Concentrations of HNO_3 exceed 1 ppbv

over the industrialized areas such as Europe, North America, central and eastern Asia, and over biomass burning regions in the tropics, in agreement with the distributions and magnitudes reported in Liao et al. (2003). Over South Asia, simulated HNO_3 concentrations are high (0.3–1 ppbv) in the northern Indian subcontinent, because the emissions of NO_x and NH_3 are high in this region (Streets et al., 2003; Zhang et al., 2009; Datta et al., 2012).

Figures 4(a)-4(b) show the simulated HNO_3 concentrations in the UTLS averaged over June-August of 2005. Since the tropopause is located at 70–150 hPa (12–15 km) over the TP/SASM region (Li et al., 2005; Bian et al., 2011b; Fadnavis et al., 2014), we choose the vertical layers of 200 hPa and 100 hPa to represent the UTLS. At both 200 hPa and 100 hPa, the highest HNO_3 concentrations are simulated to occur in the high latitude regions in the Northern Hemisphere (NH) (Fig. 4(a) and Fig. 4(b)). Simulated HNO_3 concentrations at 100 hPa are low over the region of 40–100°E and 10–30°N, which is part of the anticyclone region defined in Fig. 1. Figure 4(c) shows the latitude-altitude cross section of simulated seasonal mean HNO_3 mixing ratios averaged over 70–105°E. In boreal summer, the highest HNO_3 mixing ratios are simulated to occur at 30 hPa over the Polar Regions in both hemispheres. Over high latitudes, HNO_3 concentrations in the Southern Hemisphere (SH) are simulated to be higher than those in the NH.

To evaluate the simulated HNO_3, Figures 4(d)-4(f) show HNO_3 concentrations in the UTLS from MLS that are averaged over June-August of 2005. At 200 and 100 hPa altitudes, the observed HNO_3 mixing ratios are high in the high latitudes in the NH, which are captured by the GEOS-Chem model. The observed HNO_3 at 100 hPa exhibits low values of less than 400 pptv over

299 30–100°E and 10–30°N in the Asian monsoon anticyclone region (Fig. 4(e)). At
300 100 hPa, the observed HNO_3 mixing ratio averaged over the TP/SASM region
301 (70–105°E, 10–40°N) is 301.3 pptv, which is lower than the simulated value of
302 349.1 pptv. The difference between the simulated and observed HNO_3 mixing
303 ratio lies within the confidence range of ±500–1000 pptv of the MLS
304 instruments (Livesey et al., 2011). Considering all the grid cells with MLS
305 HNO_3 data available, the simulated seasonal mean HNO_3 concentrations show
306 normalized mean bias (NMB) of +15.9% at 100 hPa over the TP/SASM region
307 in summer of year 2005. The observed pattern of the HNO_3 vertical distribution
308 (Fig. 4(f)) is also captured by the GEOS-Chem model (Fig. 4(c)). The
309 distributions of HNO_3 in the UTLS are associated with the Brewer-Dobson (BD)
310 circulation proposed by Brewer (1949) and Dobson (1956), traveling upwards
311 across the tropopause to the stratosphere at the equator and downwards to
312 the troposphere near the Polar region.

313 **3.2 O_3**

314 Figure 3(b) shows the global distribution of simulated summertime
315 surface-layer O_3 concentrations. Simulated O_3 concentrations are in a range of
316 40–70 ppbv over Europe, North America, China, and the biomass burning
317 region of South Africa. Our model results agree closely with the simulated
318 distributions and magnitudes reported in Mickley et al. (1999), Collins et al.,
319 (2000), Liao et al. (2003), Wu et al., (2008), Zeng et al. (2008), and Fadnavis et
320 al. (2014). Fadnavis et al. (2014) also presented aircraft measurements over
321 India in September of 2010 during the Cloud Aerosol Interaction and
322 Precipitation Enhancement Experiment (CAIPEEX). Our simulated O_3
323 concentrations of 30–40 ppbv over India agree with the CAIPEEX

measurements.

Figures 5(a)-5(b) show the simulated O_3 concentrations in the UTLS averaged over June-August of 2005. The distributions of O_3 concentrations in the UTLS are similar to those of HNO_3, with elevated values in the high latitudes of the NH. Relatively low O_3 mixing ratios of less than 200 ppbv are simulated at 100 hPa over 10–30°N, 20–110°E, within the anticyclone region defined in Fig. 1. Our simulated distributions and magnitudes of O_3 agree with those reported in Bian et al. (2011b), which examined the summertime distributions of O_3 in the UTLS during 2005–2009 by using the MLS version 2.2 level 2 products (Livesey et al., 2008). Because the background O_3 concentrations are generally high in the UTLS and the stratosphere, the low O_3 concentrations in the UTLS over the TP/SASM region are caused by the deep convection that transports O_3-poor air upward (Fu et al., 2006; Randel and Park, 2006; Park et al., 2007; Bian et al., 2011b). Figure 5(c) displays the latitude-altitude cross section of seasonal mean O_3 mixing ratios averaged over 70–105°E. As a result of the BD circulation, O_3 concentrations in the UTLS are lower over the tropics than in the Polar Regions, even though the maximum O_3 concentrations are located around 10 hPa over the tropics (Brewer, 1949). Our simulated O_3 concentrations in the UTLS agree well with the measurements from MLS (Fig. 5(d)-5(f)). At 100 hPa, simulated and MLS observed O_3 mixing ratios averaged over the TP/SASM region (70–105°E, 10–40°N) are 190.6 and 145.1 ppbv, respectively. Compared to MLS observations, simulated O_3 concentrations at 100 hPa have a NMB of +31.4% over the TP/SASM region in summer of 2005. Our simulated global STE of O_3 is 420 Tg yr^{-1}, which is within the range reported in previous studies (475±120

Tg yr^{-1} in McLinden et al. (2000), 420 Tg yr^{-1} in Škerlak et al. (2014), 556±154 Tg yr^{-1} in Stevenson et al. (2006), and 550±140 Tg yr^{-1} in Solomon et al. (2007)).

In addition to the comparisons against MLS products, the simulated O_3 profiles are compared with balloon-borne sonde measurements in Fig. 6. The measurements were carried out at Kunming (KM, 102.7°E, 25.0°N) in August of 2009 and 2012, and at Lhasa (LH, 91.1°E, 29.7°N) in August of 2010 and 2013. The uncertainties of the observed O_3 mixing ratios were estimated to be within 5–10% (Bian et al. 2012). The comparisons with multi-year observations show that the model can reproduce the vertical distributions of O_3 in Kunming and Lhasa. At 100 hPa, the simulated monthly mean O_3 mixing ratio in KM is 112.6 ppbv, and the observed value is 124.2 ppbv in 2009 and 113.5 ppbv in 2012. In LH, the simulated monthly O_3 mixing ratio at 100 hPa is 152.6 ppbv, and the observed O_3 mixing ratio at that altitude is 142.4 ppbv in 2010 and 167.9 ppbv in 2013. The magnitudes of O_3 mixing ratios from these balloon-borne sonde measurements support those from MLS; O_3 mixing ratios in the UTLS are less than 200 ppbv over the TP/SASM region.

4 Simulated aerosols and model evaluation

4.1 Simulated aerosols

Figure 7 (a) shows the simulated surface-layer concentrations of SO_4^{2-}, NO_3^-, NH_4^+, OC, BC, and $PM_{2.5}$ (the sum of the mass of SO_4^{2-}, NO_3^-, NH_4^+, BC, and OC aerosols) averaged over June-August of year 2005. As expected, simulated aerosol concentrations are high over polluted regions such as India and eastern China as a result of the high anthropogenic emissions of aerosol

precursors and aerosols (Streets et al., 2003; Huang et al., 2012). Over the TP/SASM region (70–105°E, 10–40°N), the average concentrations of SO_4^{2-}, NO_3^-, NH_4^+, BC, and OC are 1.70, 0.94, 0.85, 0.30, and 0.94 μg m^{-3}, respectively. NO_3^- is simulated to be of secondary importance at the surface over the region of our interest. The simulated distributions and magnitudes of these aerosol species are similar to those reported in Wang et al. (2013) and Mu and Liao (2014).

Figures 7(b) and 7(c) also show the simulated concentrations of SO_4^{2-}, NO_3^-, NH_4^+, OC, BC, and $PM_{2.5}$ in the UTLS. Elevated concentrations of SO_4^{2-}, NO_3^-, NH_4^+, OC, BC and $PM_{2.5}$ are simulated over the TP and Plateau south slope at 200 hPa altitude, and extend from eastern Mediterranean to western China at 100 hPa. The simulated enhanced concentrations of SO_4^{2-}, OC, and BC at 100 hPa over the anticyclone region (20–120°E, 10–40°N) agree with previous observational and modeling studies (Lelieveld et al., 2001; Li et al., 2005; Fadnavis et al., 2013). Li et al. (2005) reported elevated CO concentrations in the upper troposphere over the TP, on the basis of both MLS measurements and the GEOS-Chem simulation for September 2004. Fadnavis et al. (2013) also simulated maximum concentrations of SO_4^{2-}, OC, BC, and mineral dust aerosols in the UTLS during the Asian summer monsoon season owing to convective uplifting of the boundary layer pollutants. With NO_3^- aerosol accounted for in our simulation, NO_3^- is simulated to be the most dominant aerosol species in the UTLS over the TP/SASM region, followed by SO_4^{2-}, NH_4^+, OC, and BC. At 100 hPa, the averaged concentrations of SO_4^{2-}, NO_3^-, NH_4^+, OC, and BC over the TP/SASM region (70–105°E, 10–40°N) region are 0.026, 0.069, 0.014, 0.011, and 0.002 μg m^{-3}, respectively.

4.2 Comparisons of simulated aerosol concentrations with in-situ observations

The simulated aerosol concentrations in East Asia in the GEOS-Chem model have been evaluated in previous studies (L. Zhang et al., 2010; Fu et al., 2012; Jeong and Park, 2013; Jiang et al., 2013; Wang et al., 2013; Lou et al., 2014). Here we are focused on the evaluation of aerosols in the South Asian monsoon region. For lack of publicly accessible in situ measurements of summertime aerosols in South Asia monsoon area, we compiled monthly or seasonal mean measured concentrations of each aerosol species based on measurements reported in the literature (see Table S1 in the Supplementary Material). These measurements were carried out over years of 1992–2010. The locations of sites with measurements available are shown in Fig. 8(a). Most sites are located in the upwind directions of the TP, with pollutants that can be transported to the UTLS during the South Asian summer monsoon season. The observed PM_{10} concentrations listed in Table S1 are multiplied by 0.6 to convert to $PM_{2.5}$ for model evaluation, following the suggestions in Zhang et al. (2002) and Chatterjee et al. (2010).

Figures 8(b)–8(f) show the scatterplots of simulated versus observed seasonal mean aerosol concentrations. Compared with measurements, simulated SO_4^{2-}, NO_3^-, NH_4^+, OC and BC have NMBs of –17.0%, +38.8%, +42.0%, –69.7% and –41.0%, respectively, as the concentrations of all seasons are considered. The correlations between model results and observations have *R* values of 0.49–0.85 for all aerosol species, indicating that the model is capable of capturing the spatial distributions and seasonal variations of each aerosol species in the South Asian monsoon region despite

the biases in concentrations. If we consider simulated and measured concentrations for JJA alone, the simulated concentrations of SO_4^{2-}, NO_3^-, NH_4^+, OC and BC exhibit seasonal NMBs of −14.7%, +51.5%, +74.9%, −57.2% and −32.2%, respectively, and the values of *R* are in the range of 0.24–0.85. Note that the measurements of NO_3^- and NH_4^+ are quite limited in terms of the number of samples, and the discrepancies between model results and measurements may also arise from the mismatch of the model year 2005 with the years of 1992–2010 with observations available.

4.3 Comparisons of simulated aerosol extinction coefficients with SAGE II datasets

Satellite datasets from the Stratospheric Aerosol and Gas Experiment II (SAGE II, https://eosweb.larc.nasa.gov/project/sage2/sage2_v620_table) are used to evaluate the simulated aerosol extinction in the UTLS. The SAGE II instrument was launched in October 1984 aboard the Earth Radiation Budget Satellite (ERBS) and terminated on 8 September 2005 (McCormick et al. 1987; Chu et al. 1989). The datasets used here are aerosol extinction coefficients at 525 nm from the version 6.20 SAGE retrievals, covering from 0.5 to 40 km with a vertical resolution of 0.5 km. Many validation studies have been conducted on the SAGE II aerosol data (Russell and McCormick, 1989; Oberbeck et al., 1989; Wang et al., 1989), which indicated that extinction coefficients have uncertainties of 20–30%. The extinction coefficients of aerosols in the GEOS-Chem model are calculated using aerosol mass concentration, extinction efficiency, effective radius, particle mass density, and the assumed aerosol size distribution (Drury et al., 2010). The hygroscopic growth of each aerosol species with relative humidity is accounted for, using the hygroscopic

growth factors listed in Martin et al. (2003).

Figure 9(a) presents the simulated monthly mean distribution of aerosol extinction coefficients at 100 hPa for July of 2005. At 100 hPa, the simulated aerosol extinction coefficients are relatively high over the anticyclone region, where anthropogenic aerosol species (Fig. 7) and natural aerosols such as mineral dust and sea salt contribute to aerosol extinction coefficients in summer. Note that the contributions of sulfate, nitrate, ammonium, OC, sea salt, and mineral dust are all considered when we calculate aerosol extinction coefficients. Aerosol extinction coefficients are simulated to be $1.2–2\times10^{-3}$ km^{-1} at 100 hPa over the Asian continent and Indian Ocean (20°S–30°N, 30°–105°E). These values agree closely with aerosol extinction coefficients measured at Naqu during August of 2011 for the same altitude, the maximum of which was 2.4×10^{-3} km^{-1} (He et al., 2014). Vernier et al. (2011) also identified this Asian aerosol layer with high SR at 100 hPa by observations of CALIPSO for JJA of 2006–2008.

Figure 9(b) displays the monthly mean vertical profiles of aerosol extinction coefficients averaged over the Asian monsoon anticyclone region (20–120°E 10–40°N) (Fig. 1) for July of 2005. The SAGE II datasets are available for July only in 2005. The profiles from SAGE II and the GEOS-Chem simulation are all shown. Accounting for all aerosol species, the GEOS-Chem model reproduces well the aerosol extinction coefficients above 10 km, but the discrepancies are rather large in altitudes less than 10 km. Note that the uncertainties in satellite datasets increase as the altitude decreases (Vanhellemont et al., 2008； Kulkarni and Ramachandran, 2015), and the missing data in the lower troposphere along the satellite trajectories over the region of our interest also

474 contribute to the discrepancies

475 Comparisons of profiles of aerosol extinction coefficients with and without
476 nitrate aerosol indicate that the profiles show small differences in altitudes less
477 than 6 km but large discrepancies from 6 km to the tropopause. With nitrate
478 aerosol accounted for, the simulated aerosol extinction coefficients agree
479 closely with SAGE II datasets in the UTLS (averaged over 14–16 km, the
480 simulated value is 8.6×10^{-4} km^{-1} while the observed value is 8.0×10^{-4} km^{-1}).
481 Without nitrate aerosol, the simulated aerosol extinction coefficient at 14–16
482 km altitude is 1.5×10^{-4} km^{-1}, which underestimates the aerosol extinction
483 coefficient by 82.6% compared to that calculated with all the aerosol species.
484 These comparisons of extinction coefficients with and without nitrate aerosol
485 suggest that nitrate aerosol plays an important role in aerosol extinction in the
486 UTLS over the region of our interest.

487

488 **5 Contribution of nitrate to aerosol concentrations in the UTLS**

489 Since nitrate aerosol is simulated to be the most abundant aerosol species in
490 the UTLS over the TP/SASM region, we analyze the contribution of nitrate to
491 $PM_{2.5}$ concentration (C_{NIT}=nitrate concentration/$PM_{2.5}$ concentration) in this
492 section. Figure 10 shows the simulated seasonal mean distributions of C_{NIT} for
493 June-August of year 2005. At the surface layer (Fig. 10(a)), simulated high C_{NIT}
494 values are located over the areas with high nitrate concentrations (India and
495 eastern China) as well as the oceans where NO_3^- also forms on sea salt and
496 mineral dust particles (Arimoto et al., 1996; Nakamura et al., 2005; George and
497 Nair, 2008). Over the TP/SASM region, the C_{NIT} values in JJA are 5–35% at the
498 surface, 25–50% at 200 hPa (Fig. 10(b)), and could exceed 60% at 100 hPa

499 (Fig. 10(c)). The latitude-altitude cross section of C_{NIT} (Fig. 10(d)) shows that
500 C_{NIT} over 20–40°N increases with altitude and reaches maximum values
501 around the extratropical tropopause.

502 Table 2 lists the mean concentrations of SO_4^{2-}, NO_3^-, NH_4^+, BC and OC, and
503 their contributions to $PM_{2.5}$ during summertime of 2005 over the TP/SASM, TP,
504 and SASM regions. Over the TP/SASM region, SO_4^{2-}, NO_3^-, NH_4^+, BC and OC
505 are simulated to contribute 35.9%, 19.8%, 18.1%, 6.4%, and 19.8%,
506 respectively, to $PM_{2.5}$ mass concentration at the surface layer. The
507 contributions increase significantly in the UTLS. The largest C_{NIT} is simulated
508 in the SASM region at 100 hPa, where NO_3^- accounts for 60.5% of $PM_{2.5}$ mass
509 concentration. The high C_{NIT} values indicate that NO_3^- plays an important role
510 in the aerosol layer in the UTLS over the TP/SASM region.

511

512 **6 Mechanisms for high nitrate concentrations in the UTLS**

513 **6.1 Upward transport of nitrate from the lower troposphere**

514 The intense convective transport of chemical species into the UTLS over the
515 TP/SASM region during summertime has been widely discussed in previous
516 studies (Randel et al., 2010; Bian et al., 2011a; Fadnavis et al., 2013, 2014;
517 Qie et al., 2014; He et al., 2014). Since nitrate aerosol is simulated to be of
518 secondary abundant aerosol species in the surface layer over the TP/SASM
519 region (Fig. 7), the vertical mass transport through the deep convection in this
520 region contributes to the accumulation of NO_3^- in the UTLS. Figure 11 shows
521 the latitude-altitude cross sections of simulated concentrations of SO_4^{2-} and
522 NO_3^- averaged over 70–105°E in June-August of 2005, together with the
523 wind vectors obtained from the European Centre for Medium-Range Weather

Forecasts (ECMWF) ERA-Interim Reanalysis data. Note that the assimilated GEOS-5 meteorological fields do not have vertical winds (http://wiki.seas.harvard.edu/geos-chem/index.php/List_of_GEOS-5_met_fields), so we use the ECMWF reanalysis wind fields to do the analysis here. High values of aerosol concentrations are found on the south slope of the Himalayas, where the deep convection exists. Although both SO_4^{2-} and NO_3^- are transported upward to the extratropical tropopause, the details of the vertical distributions are different. At altitudes higher than 8 km, the concentrations of NO_3^- do not decrease with altitude as quickly as those of SO_4^{2-}, and the concentrations of NO_3^- over 10–40°N are higher than those of SO_4^{2-}.

The chemical mechanisms for the formation of SO_4^{2-}, NO_3^-, and NH_4^+ aerosols in the GEOS-Chem model were described in R. J. Park et al. (2004), which are comprehensive and have been used extensively in previous studies to simulate these three aerosol species (R. J. Park et al., 2004; Pye et al., 2009; L. Zhang et al., 2010; Zhu et al., 2012; Jiang et al., 2013; Lou et al., 2014). Sulfate aerosol forms from gas-phase oxidation of SO_2 by OH and from in-cloud oxidation of SO_2 by O_3 and H_2O_2. Nitrate forms from the partitioning of HNO_3 between gas and aerosol phases, which is calculated by the ISORROPIA II thermodynamic equilibrium module (Fountoukis and Nenes, 2007) in the GEOS-Chem model. Major reactions for the production and loss of HNO_3 were listed in Liao and Seinfeld (2005). HNO_3 is produced by the reaction of NO with OH during daytime and by hydrolysis of N_2O_5 on aerosol surfaces at night. The chemical mechanisms for SO_4^{2-} and NO_3^- have different sensitivity to meteorological conditions. During the vertical transport,

549 temperature decreases, which reduces the gas-phase oxidation of SO_2 (Yao et
550 al., 2002; Seinfeld and Pandis 2006; X. Y. Zhang et al., 2012) but promotes the
551 formation of NO_3^- by shifting gas-particle equilibria (Dawson et al., 2007; Liao
552 et al., 2009). Therefore the different chemical mechanisms for $SO_4^{2-}$and NO_3^-
553 formation contribute to the differences in their vertical distributions.

554 **6.2 The gas-to-aerosol conversion of HNO_3 to form nitrate**

555 As mentioned above, the formation of gas-phase HNO_3 and the partitioning of
556 HNO_3 between gas and aerosol phases are the two major chemical processes
557 that influence NO_3^- concentrations. We have evaluated the ability of the
558 GEOS-Chem model to simulate gas-phase HNO_3 in Section 3.1 (by
559 comparisons of our model results with MLS observations and concentrations
560 from previous modeling studies), so we quantify here NO_3^- formation from
561 gas-to-aerosol conversion of HNO_3 based on the ISORROPIA II
562 thermodynamic equilibrium module (Fountoukis and Nenes, 2007). The
563 gas-to-aerosol conversion of HNO_3 to form NO_3^- is very sensitive to relative
564 humidity (RH) and temperature (Fountoukis and Nenes 2007; Dawson et al.,
565 2007). Low temperature and high RH are favorable for NO_3^- formation. Figure
566 12 shows the seasonal mean horizontal distributions of RH and temperature at
567 100 hPa and the latitude-altitude cross sections of these two parameters
568 averaged over 70–105°E. RH exhibits high values in the TP/SASM region,
569 which are consistent with the high H_2O mixing ratios in this area reported in
570 Gettelman et al. (2004), M. Park et al. (2004), and Fu et al. (2006). At 100 hPa,
571 the locations with high RH of exceeding 45% correspond well with those with
572 high C_{NIT} values (Fig. 10(c)). The latitude-altitude cross section of RH (Fig.
573 12(c)) shows that RH has high values over the places with intense upward

574 transport (Fig. 11). For temperature, as Fig. 12(b) and 12(d) show, summertime
575 temperatures are cold (190–200 K) at 100 hPa in the TP/SASM region,
576 consistent with the distribution and magnitude reported for August, 2011, in He
577 et al. (2014) on the basis of the NCEP Reanalysis data. The low temperatures
578 over the TP/SASM region are associated with the adiabatic expansion of
579 ascending air mass of the deep convections (Yanai et al., 1992; Park et al.,
580 2007; He et al., 2014).

581 Because of the favorable conditions of RH and temperature, the
582 gas-to-aerosol conversion of HNO_3 to form nitrate can occur during the upward
583 transport and in the UTLS. Figure 13 shows the mass budget for nitrate
584 aerosol within the selected box of (70–105°E, 10–40°N, 8–16 km) to see the
585 role of nitrate formation over the TP/SASM region. The horizontal mass fluxes
586 have a net negative value of 0.10 Tg season^{-1}, reducing nitrate aerosol in the
587 selected box. The vertical transport and the gas-to-aerosol conversion of
588 HNO_3 increase nitrate mass in the selected box, with values of 0.09 Tg
589 season^{-1} and 0.11 Tg season^{-1}, respectively, indicating that the gas-to-aerosol
590 conversion plays an important role in the enhancement of nitrate in the UTLS
591 over the TP/SASM region. Although relatively high RH exists near the
592 tropopause of the TP/SASM region, the air near the tropopause is still dryer
593 compared to that in the lower altitudes. Model results show that the
594 gas-to-aerosol partition of HNO_3 decreases with altitude over 8–16 km,
595 indicating that the gas to aerosol conversion contributes to nitrate
596 accumulation in the UTLS mainly during the process of upward transport.

597 Previous studies have also reported that nitric acid trihydrates (NAT,
598 $HNO_3 \bullet (H_2O)_3$) could form in the polar and tropical stratosphere at low

599 temperatures through two mechanisms: (1) the homogeneous nucleation out
600 of supercooled ternary solutions, and (2) the heterogeneous formation on ice
601 particles (Hofmann et al., 1989; Carslaw et al., 1998; Voigt et al., 2000; Popp et
602 al., 2006; Kirner et al., 2011). A typical NAT condensation temperature is
603 approximate 193 K (Kirner et al., 2011). As shown in Fig. 12, the temperatures
604 around 100 hPa over the TP/SASM region are in the range of 190–200 K,
605 which are low enough to produce some NAT particles. However, balloon-borne
606 measurements of depolarization ratio and backscattering ratio of aerosols at
607 Lhasa during August-October of 1999 by Kim et al. (2003) and Tobo et al.
608 (2007) suggested that coarse and aspherical particles such as NAT are scarce
609 in the UTLS of the TP/SASM.
610
611 **7 Impacts of uncertainties in surface-layer aerosol concentrations on**
612 **simulated nitrate in the UTLS**
613 Since simulated SO_4^{2-}, NO_3^- and NH_4^+ concentrations have, respectively,
614 NMBs of –17.0%, +38.8%, and +42.0% on an annual mean basis and of
615 –14.7%, +51.5%, and +74.9% in summer (Section 4.2), we perform four
616 sensitivity simulations to examine the impacts of uncertainties in surface-layer
617 aerosol concentrations on simulated nitrate in the UTLS. In the first three
618 cases, anthropogenic emissions of NO_x, NH_3, and SO_2 in Asia are changed by
619 –50%, –50%, and +20%, respectively, relative to those in our standard
620 simulation. In the last case, anthropogenic emissions of all these three species
621 are changed simultaneously, with NO_x reduced by 50%, NH_3 reduced by 50%,
622 and SO_2 increased by 20% in Asia relative to the standard case. The purpose
623 of these sensitivity studies is to reduce NMBs of simulated surface-layer

concentrations of SO_4^{2-}, NO_3^- and NH_4^+ and see whether NO_3^- is still the most dominant aerosol species in the UTLS. Model results from these sensitivity studies for summer of 2005 are presented in Table 3.

As anthropogenic emissions of SO_2 in Asia are increased by 20%, the NMB of simulated surface-layer SO_4^{2-} concentrations is –4.4%, which is an improvement compared to the NMB of –14.7% in the standard simulation. However, the increases in SO_2 emissions lead to larger NMBs of surface-layer NO_3^- and NH_4^+ because of the increased formation of ammonium sulfate or ammonium bisulfate. The percentage contributions of SO_4^{2-} to total aerosol mass in the UTLS increase slightly by 2.7% at 200 hPa and by 1.6% at 100 hPa, and nitrate in the UTLS also shows small sensitivity to the change in SO_2 emissions.

With anthropogenic emissions of NO_x in Asia reduced by 50%, the NMB of simulated surface-layer NO_3^- concentrations changes from +51.5% in the standard simulation to –11.7% in this sensitivity run. The contribution of each of SO_4^{2-}, NO_3^- and NH_4^+ aerosols to total aerosol mass in the UTLS is not sensitive to this reduction in NO_x emissions at the surface; the percentage contribution obtained from this sensitivity run is very close to the value obtained in the standard simulation (Table 3). Similarly, in the sensitivity study with NH_3 emissions reduced by 50% in Asia, simulated surface-layer concentrations of NO_3^- and NH_4^+ are improved in terms of the values of NMBs, but the improvement in simulated aerosol concentrations at the surface-layer does not influence our conclusion of high nitrate aerosol concentration in the UTLS.

In the sensitivity study with emissions of NO_x, NH_3, and SO_2 in Asia

649 changed simultaneously, simulated surface-layer concentrations of SO_4^{2-}, NO_3^-
650 and NH_4^+ have NMBs of −8.3%, −27.0% and +55.4%, respectively, which are
651 all improved compared to those in the standard simulation. Even though nitrate
652 aerosol is now underestimated at the surface, it still accounts for 53.3% of the
653 $PM_{2.5}$ concentration at 100 hPa over the TP/SASM region in summer.

654 It should be noted that the concentrations of OC and BC are also
655 underestimated, with NMBs of −57.2% and −32.2%, respectively, in summer
656 (Section 4.2). We have done a simple calculation with the concentrations of
657 OC and BC in the UTLS multiplied by 2.3 and 1.5, respectively, and nitrate is
658 still the most dominant aerosol species in summertime in the UTLS over the
659 TP/SASM region (not shown in Table 3). Therefore the uncertainties in surface
660 aerosol concentrations do not compromise the conclusion of this study.

661

662 **8 Conclusions**

663 In this work we simulate nitrate aerosol and its contribution to aerosol
664 concentrations in the UTLS over the TP/SASM region (70–105°E, 10–40°N)
665 for summertime of year 2005, using the global chemical transport model
666 GEOS-Chem driven by the assimilated meteorological fields.

667 Simulated HNO_3 and O_3 are evaluated to show the model's ability to
668 simulate the NOx-O_3-HNO_3 cycle over the studied region. In the UTLS, both
669 the horizontal and vertical distributions of simulated HNO_3 and O_3 agree well
670 with the MLS observations. At 100 hPa, simulated seasonal mean HNO_3 and
671 O_3 mixing ratios show NMBs of +15.9% and +31.4%, respectively, over the
672 TP/SASM region (70−105°E, 10−40°N) in summer of year 2005, and the model
673 biases lie within the confidence range of the MLS instruments. Both simulated

674 and observed O_3 concentrations show relatively low values of less than 200
675 ppbv at 100 hPa over the TP/SASM region.

676 Averaged over the TP/SASM region, the surface-layer concentrations of
677 SO_4^{2-}, NO_3^-, NH_4^+, BC, and OC are simulated to be 1.70, 0.94, 0.85, 0.30, and
678 0.94 μg m^{-3}, respectively. Nitrate aerosol is simulated to be of secondary
679 importance near the surface over the region of our interest. Comparisons of
680 simulated aerosol concentrations with ground-based observations show that
681 simulated summertime concentrations of SO_4^{2-}, NO_3^-, NH_4^+, OC and BC have
682 NMB of −14.7%, +51.5%, +74.9%, −57.2% and −32.2%, respectively. Note that
683 the measurements of NO_3^- and NH_4^+ are quite limited in terms of the number
684 of samples.

685 Model results show elevated concentrations of SO_4^{2-}, NO_3^-, NH_4^+, OC, BC
686 and $PM_{2.5}$ in the UTLS over the TP/SASM region throughout the summer. NO_3^-
687 is simulated to be the most dominant aerosol species in the UTLS of the
688 TP/SASM region. Accounting for NO_3^- aerosol, the GEOS-Chem model
689 reproduces well the magnitude of aerosol extinctions above 10 km, as model
690 results are compared with the SAGE II measurements. The discrepancies
691 between the simulated and observed aerosol extinction coefficient are within 8%
692 in the UTLS (averaged over 14–16 km). Simulated vertical profiles of aerosol
693 extinction coefficients with and without nitrate aerosol show large
694 discrepancies from 6 km to tropopause, indicating the important role of nitrate
695 in aerosol layer in the UTLS over the TP/SASM region.

696 The contribution of NO_3^- to aerosols in the TP/SASM region is quantified
697 by C_{NIT} (the ratio of nitrate concentration to $PM_{2.5}$ concentration). Over the
698 TP/SASM region, the C_{NIT} values in summer are 5–35% at the surface, 25–

699 50% at 200 hPa, and could exceed 60% at 100 hPa. The mechanisms for the
700 accumulation of nitrate in the UTLS over the TP/SASM region include vertical
701 transport and the gas-to-aerosol conversion of HNO_3 to form nitrate. Such
702 gas-to-aerosol conversion occurs during the upward transport and in the UTLS.
703 The high relative humidity and low temperature associated with the deep
704 convection over the TP/SASM region are favorable for nitrate formation.

705 Results from the present study indicate that nitrate is an important aerosol
706 species in the UTLS over the ASM/TP region. Considering the scarce
707 measurements of nitrate in the UTLS and the model uncertainties, more
708 observational and modeling studies are needed to further explore the aerosol
709 composition in the Asian tropopause aerosol layer. Further simulations of
710 nitrate aerosol in the UTLS also need to account for NAT formation at low
711 temperatures (Kirner et al., 2011) and the roles of natural aerosols, including
712 the transport of mineral dust and sea salt to the UTLS as well as nitrate
713 formation on these natural particles (Ma et al., 2003).

714

715

716 *Acknowledgments.* This work was supported by the National Basic Research
717 Program of China (973 program, Grant No. 2014CB441202), the Strategic
718 Priority Research Program of the Chinese Academy of Sciences (Grant No.
719 XDA05100503), and the National Natural Science Foundation of China under
720 grants 41021004, 41475137, and 91544219. We gratefully acknowledge
721 NASA, USA, for providing the MLS and SAGE II data on their website.

722

723 **References**

724 Adhikary, B., Carmichael, G. R., Tang, Y., Leung, L. R., Qian, Y., Schauer, J. J.,
725 Stone, E. A., Ramanathan, V., and Ramana, M. V.: Characterization of the
726 seasonal cycle of south Asian aerosols: A regional-scale modeling
727 analysis, J. Geophys. Res., 112, D22S22, doi:10.1029/2006JD008143,
728 2007.
729 Alexander, B., Park, R. J., Jacob, D. J., Li, Q., Yantosca, R. M., Savarino, J.,
730 Lee, C., and Thiemens, M.: Sulfate formation in sea-salt aerosols:
731 Constraints from oxygen isotopes, J. Geophys. Res., 110, D10307,
732 doi:10.1029/2004JD005659, 2005.
733 Arimoto, R., Duce, R., Savoie, D., Prospero, J., Talbot, R., Cullen, J., Tomza,
734 U., Lewis, N., and Ray, B.: Relationships among aerosol constituents from
735 Asia and the North Pacific during PEM–West A, J. Geophys. Res., 101,
736 2011–2023, 1996.
737 Babu, S. S. and Moorthy, K. K.: Aerosol black carbon over a tropical coastal
738 station in India, Geophys. Res. Lett., 29, 2098,
739 doi:10.1029/2002GL015662, 2002.
740 Bano, T., Singh, S., Gupta, N., Soni, K., Tanwar, R., Nath, S., Arya, B., and
741 Gera, B.: Variation in aerosol black carbon concentration and its emission
742 estimates at the mega-city Delhi, Int. J. Remote Sens., 32, 6749–6764,
743 2011.
744 Bian, J., Yan, R., and Chen, H.: Tropospheric Pollutant Transport to the
745 Stratosphere by Asian Summer Monsoon, Chinese Journal of
746 Atmospheric Sciences, 35, 897–902, 2011a.
747 Bian, J., Yan, R., Chen, H., Lü, D., and MASSIE, S. T.: Formation of the
748 Summertime Ozone Valley over the Tibetan Plateau: The Asian Summer
749 Monsoon and Air Column Variations, Adv. Atmos. Sci., 28, 1318–1325,
750 2011b.
751 Bian, J., Pan, L. L., Paulik, L., Vömel, H., Chen, H., and Lü, D.: In situ water
752 vapor and ozone measurements in Lhasa and Kunming during the Asian
753 summer monsoon, Geophys. Res. Lett., 39, L19808,
754 doi:10.1029/2012GL052996, 2012.
755 Bourgeois, Q., Bey, I., and Stier, P.: A permanent aerosol layer at the tropical
756 tropopause layer driven by the intertropical convergence zone, Atmos.
757 Chem. Phys. Discuss., 12, 2863–2889, 2012.
758 Bouwman, A., Lee, D., Asman, W., Dentener, F., Van Der Hoek, K., and Olivier,
759 J.: A global high-resolution emission inventory for ammonia, Global
760 Biogeochem. Cy., 11, 561-587, 1997.
761 Brewer, A. W.: Evidence for a world circulation provided by the measurements
762 of helium and water vapour distribution in the stratosphere, Q. J. Roy.
763 Meteor. Soc., 75, 351-363, 1949.
764 Carrico, C. M., Bergin, M. H., Shrestha, A. B., Dibb, J. E., Gomes, L., and
765 Harris, J. M.: The importance of carbon and mineral dust to seasonal
766 aerosol properties in the Nepal Himalaya, Atmos. Environ., 37, 2811–2824,
767 2003.
768 Carslaw, K., Wirth, M., Tsias, A., Luo, B., Dörnbrack, A., Leutbecher, M.,
769 Volkert, H., Renger, W., Bacmeister, J., and Peter, T.: Particle
770 microphysics and chemistry in remotely observed mountain polar
771 stratospheric clouds, J. Geophys. Res., 103, 5785–5796, 1998.
772 Chatterjee, A., Adak, A., Singh, A. K., Srivastava, M. K., Ghosh, S. K., Tiwari,
773 S., Devara, P. C., and Raha, S.: Aerosol chemistry over a high altitude

774 station at northeastern Himalayas, India, PloS one, 5, e11122,
775 doi:10.1371/journal.pone.0011122, 2010.
776 Chatterjee, A., Ghosh, S. K., Adak, A., Singh, A. K., Devara, P. C., and Raha,
777 S.: Effect of Dust and Anthropogenic Aerosols on Columnar Aerosol
778 Optical Properties over Darjeeling (2200 m asl), Eastern Himalayas, India,
779 PloS one, 7, e40286, doi:10.1371/journal.pone.0040286, 2012.
780 Chen, H., Bian, J., and Lü, D.: Advances and prospects in the study of
781 stratosphere-troposphere exchange, Chinese J. Atmos. Sci., 30, 813–820,
782 doi:1006-9895(2006)30:5<813:SDLCXP>2.0.TX;2-A, 2006.
783 Chowdhury, Z., Zheng, M., Schauer, J. J., Sheesley, R. J., Salmon, L. G., Cass,
784 G. R., and Russell, A. G.: Speciation of ambient fine organic carbon
785 particles and source apportionment of $PM_{2.5}$ in Indian cities, J. Geophys.
786 Res., 112, D15303, doi:10.1029/2007JD008386, 2007.
787 Chu, W., McCormick, M., Lenoble, J., Brogniez, C., and Pruvost, P.: SAGE II
788 inversion algorithm, J. Geophys. Res., 94, 8339–8351, 1989.
789 Collins, W. J., Stevenson, D. S., Johnson, C. E., and Derwent, R. G.: The
790 European regional ozone distribution and its links with the global scale for
791 the years 1992 and 2015, Atmos. Environ., 34, 255–267, 2000.
792 Considine, D. B., Rosenfield, J. E., and Fleming, E. L.: An interactive model
793 study of the influence of the Mount Pinatubo aerosol on stratospheric
794 methane and water trends, J. Geophys. Res., 106, 27711-27727,
795 doi:10.1029/2001jd000331, 2001.
796 Considine, D. B., Logan, J. A., and Olsen, M. A.: Evaluation of
797 near-tropopause ozone distributions in the Global Modeling Initiative
798 combined stratosphere/troposphere model with ozonesonde data, Atmos.
799 Chem. Phys., 8, 2365–2385, 2008.
800 Datta, A., Sharma, S., Harit, R., Kumar, V., Mandal, T., and Pathak, H.:
801 Ammonia emission from subtropical crop land area in India, Asia-Pac. J.
802 Atmos. Sci., 48, 275–281, 2012.
803 Dawson, J., Adams, P., and Pandis, S.: Sensitivity of $PM_{2.5}$ to climate in the
804 Eastern US: a modeling case study, Atmos. Chem. and phys., 7,
805 4295–4309, 2007.
806 Decesari, S., Facchini, M., Carbone, C., Giulianelli, L., Rinaldi, M., Finessi, E.,
807 Fuzzi, S., Marinoni, A., Cristofanelli, P., and Duchi, R.: Chemical
808 composition of PM_{10} and PM_1 at the highaltitude Himalayan station Nepal
809 Climate Observatory-Pyramid (NCO-P)(5079 m asl), Atmos. Chem. Phys,
810 10, 4583–4596, 2010.
811 Dobson, G. M. B.: Origin and distribution of the polyatomic molecules in the
812 atmosphere, Proceedings of the Royal Society of London. Series A,
813 Mathematical and Physical Sciences, 187–193, 1956.
814 Drury, E., Jacob, D. J., Spurr, R. J., Wang, J., Shinozuka, Y., Anderson, B. E.,
815 Clarke, A. D., Dibb, J., McNaughton, C., and Weber, R.: Synthesis of
816 satellite (MODIS), aircraft (ICARTT), and surface (IMPROVE, EPA–AQS,
817 AERONET) aerosol observations over eastern North America to improve
818 MODIS aerosol retrievals and constrain surface aerosol concentrations
819 and sources, J. Geophys. Res., 115, D14204, doi:10.1029/2009JD012629,
820 2010.
821 Duncan, B., Strahan, S., Yoshida, Y., Steenrod, S., and Livesey, N.: Model
822 study of the cross-tropopause transport of biomass burning pollution,
823 Atmos. Chem. Phys., 7, 3713–3736, 2007.

824 Dutkiewicz, V. A., Alvi, S., Ghauri, B. M., Choudhary, M. I., and Husain, L.:
825 Black carbon aerosols in urban air in South Asia, Atmos. Environ., 43,
826 1737–1744, 2009.
827 Evans, M., and Jacob, D. J.: Impact of new laboratory studies of N_2O_5
828 hydrolysis on global model budgets of tropospheric nitrogen oxides, ozone,
829 and OH, Geophys. Res. Lett., 32, 10 L09813, doi:10.1029/2005GL022469,
830 2005.
831 Fadnavis, S., Semeniuk, K., Pozzoli, L., Schultz, M., Ghude, S., Das, S., and
832 Kakatkar, R.: Transport of aerosols into the UTLS and their impact on the
833 Asian monsoon region as seen in a global model simulation, Atmos. Chem.
834 Phys., 13, 8771–8786, 2013.
835 Fadnavis, S., Semeniuk, K., Schultz, M., Mahajan, A., Pozzoli, L., Sonbawane,
836 S., and Kiefer, M.: Transport pathways of peroxyacetyl nitrate in the upper
837 troposphere and lower stratosphere from different monsoon systems
838 during the summer monsoon season, Atmos. Chem. Phys. Discuss., 14,
839 20159–20195, 2014.
840 Fairlie, T. D., Jacob, D. J., and Park, R. J.: The impact of transpacific transport
841 of mineral dust in the United States, Atmos. Environ., 41, 1251–1266,
842 2007.
843 Fisher, J. A., Jacob, D. J., Wang, Q., Bahreini, R., Carouge, C. C., Cubison, M.
844 J., Dibb, J. E., Diehl, T., Jimenez, J. L., and Leibensperger, E. M.: Sources,
845 distribution, and acidity of sulfate–ammonium aerosol in the Arctic in
846 winter–spring, Atmos. Environ., 45, 7301–7318, 2011.
847 Fountoukis, C., and Nenes, A.: ISORROPIA II: a computationally efficient
848 thermodynamic equilibrium model for
849 K^+–Ca^{2+}–Mg^{2+}–NH_4^+–Na^+–SO_4^{2-}–NO_3^-–Cl^-–H_2O aerosols, Atmos. Chem.
850 Phys., 7, 4639–4659, 2007.
851 Froyd, K., Murphy, D., Sanford, T., Thomson, D., Wilson, J., Pfister, L., and Lait,
852 L.: Aerosol composition of the tropical upper troposphere, Atmos. Chem.
853 Phys., 9, 4363–4385, 2009.
854 Fu, R., Hu, Y., Wright, J. S., Jiang, J. H., Dickinson, R. E., Chen, M., Filipiak,
855 M., Read, W. G., Waters, J. W., and Wu, D. L.: Short circuit of water vapor
856 and polluted air to the global stratosphere by convective transport over the
857 Tibetan Plateau, P. Natl. A. Sci., 103, 5664–5669, 2006.
858 Fu, T. -M., Cao, J., Zhang, X., Lee, S., Zhang, Q., Han, Y., Qu, W., Han, Z.,
859 Zhang, R., and Wang, Y.: Carbonaceous aerosols in China: top–down
860 constraints on primary sources and estimation of secondary contribution,
861 Atmos. Chem. Phys., 12, 2725–2746, 2012.
862 Ganguly, D., Jayaraman, A., and Gadhavi, H.: Physical and optical properties
863 of aerosols over an urban location in western India: Seasonal variabilities,
864 J. Geophys. Res., 111, D24206, doi:10.1029/2006JD007392, 2006.
865 George, S. K., and Nair, P. R.: Aerosol mass loading over the marine
866 environment of Arabian Sea during ICARB: Sea-salt and non-sea-salt
867 components, J. Earth Syst. Sci., 117, 333–344, 2008.
868 George, S. K., Nair, P. R., Parameswaran, K., Jacob, S., and Abraham, A.:
869 Seasonal trends in chemical composition of aerosols at a tropical coastal
870 site of India, J. Geophys. Res., 113, D16209, doi:10.1029/2007JD009507,
871 2008.
872 Gettelman, A., Kinnison, D. E., Dunkerton, T. J., and Brasseur, G. P.: Impact of
873 monsoon circulations on the upper troposphere and lower stratosphere, J.

874 Geophys. Res., 109, D22101, doi:10.1029/2004JD004878, 2004.
875 Guenther, A., Karl, T., Harley, P., Wiedinmyer, C., Palmer, P., and Geron, C.:
876 Estimates of global terrestrial isoprene emissions using MEGAN (Model of
877 Emissions of Gases and Aerosols from Nature), Atmos. Chem. Phys.
878 Discuss., 6, 107–173, 2006.
879 Hack, J. J.: Parameterization of moist convection in the National Center for
880 Atmospheric Research community climate model (CCM2), J. Geophys.
881 Res., 99, 5551–5568, doi:10.1029/93jd03478, 1994.
882 He, Q., Li, C., Ma, J., Wang, H., Yan, X., Liang, Z., and Qi, G.: Enhancement of
883 aerosols in UTLS over the Tibetan Plateau induced by deep convection
884 during the Asian summer monsoon, Atmos. Chem. Phys. Discuss., 14,
885 3169-3191, 10.5194/acpd–14–3169–2014, 2014.
886 Hegde, P., Sudheer, A., Sarin, M., and Manjunatha, B.: Chemical
887 characteristics of atmospheric aerosols over southwest coast of India,
888 Atmos. Environ., 41, 7751–7766, 2007.
889 Hofmann, D., Rosen, J., Harder, J., and Hereford, J.: Balloon-borne
890 measurements of aerosol, condensation nuclei, and cloud particles in the
891 stratosphere at McMurdo Station, Antarctica, during the spring of 1987, J.
892 Geophys. Res., 94, 11253–11269, doi:10.1029/JD094iD09p11253, 1989.
893 Huang, C., Chen, C. H., Li, L., Cheng, Z., Wang, H. L., Huang, H. Y., Streets, D.
894 G., and Wang, Y. J.: Emission inventory of anthropogenic air pollutants
895 and VOC species in the Yangtze River Delta region, China, Atmos. Chem.
896 Phys., 11, 4105–4120, 2011.
897 Huang, X., Song, Y., Li, M., Li, J., Huo, Q., Cai, X., Zhu, T., Hu, M., and Zhang,
898 H.: A high-resolution ammonia emission inventory in China, Global
899 Biogeochem. Cy., 26, GB1030, doi:10.1029/2011GB004161, 2012.
900 Husain, L., Dutkiewicz, V. A., Khan, A., and Ghauri, B. M.: Characterization of
901 carbonaceous aerosols in urban air, Atmos. Environ., 41, 6872–6883,
902 2007.
903 Jacob, D. J.: Heterogeneous chemistry and tropospheric ozone, Atmos.
904 Environ., 34, 2131-2159, 2000.
905 Jaeglé, L., Quinn, P., Bates, T., Alexander, B., and Lin, J.-T.: Global distribution
906 of sea salt aerosols: new constraints from in situ and remote sensing
907 observations, Atmos. Chem. Phys., 11, 3137–3157, 2011.
908 Jayaraman, A., Gadhavi, H., Ganguly, D., Misra, A., Ramachandran, S., and
909 Rajesh, T.: Spatial variations in aerosol characteristics and regional
910 radiative forcing over India: Measurements and modeling of 2004 road
911 campaign experiment, Atmos. Environ., 40, 6504–6515, 2006.
912 Jeong, J. I., and Park, R. J.: Effects of the meteorological variability on regional
913 air quality in East Asia, Atmos. Environ., 69, 46–55, 2013.
914 Jiang, H., Liao, H., Pye, H., Wu, S., Mickley, L. J., Seinfeld, J. H., and Zhang,
915 X.: Projected effect of 2000-2050 changes in climate and emissions on
916 aerosol levels in China and associated transboundary transport, Atmos.
917 Chem. Phys., 13, 7937–7960, 2013.
918 Kar, J., Bremer, H., Drummond, J. R., Rochon, Y. J., Jones, D., Nichitiu, F., Zou,
919 J., Liu, J., Gille, J. C., and Edwards, D. P.: Evidence of vertical transport of
920 carbon monoxide from Measurements of Pollution in the Troposphere
921 (MOPITT), Geophys. Res. Lett., 31, L23105, doi:10.1029/2004GL021128,
922 2004.
923 Kim, J., Song, C. H., Ghim, Y., Won, J., Yoon, S., Carmichael, G., and Woo, J.

924 H.: An investigation on NH_3 emissions and particulate $NH_4^+ - NO_3^-$
925 formation in East Asia, Atmos. Environ., 40, 2139–2150, 2006.
926 Kim, Y.- S., Shibata, T., Iwasaka, Y., Shi, G., Zhou, X., Tamura, K., and Ohashi,
927 T.: Enhancement of aerosols near the cold tropopause in summer over
928 Tibetan Plateau: lidar and balloonborne measurements in 1999 at Lhasa,
929 Tibet, China, in: Lidar Remote Sensing for Industry and Environment
930 Monitoring III, edited by: Singh U. N., Itabe, T., and Liu, Z., Proceedings of
931 SPIE, Hangzhou, China, 4893, 496–503, 2003.
932 Kirner, O., Ruhnke, R., Buchholz-Dietsch, J., Jöckel, P., Brühl, C., and Steil, B.:
933 Simulation of polar stratospheric clouds in the chemistry-climate-model
934 EMAC via the submodel PSC, Geoscientific Model Development, 4,
935 169–182, 2011.
936 Kulkarni, P., and Ramachandran, S.: Comparison of aerosol extinction
937 between lidar and SAGE II over Gadanki, a tropical station in India, Ann.
938 Geophys., 2015, 351–362,
939 Kulshrestha, U., Saxena, A., Kumar, N., Kumari, K., and Srivastava, S.:
940 Chemical composition and association of size-differentiated aerosols at a
941 suburban site in a semi-arid tract of India, J. Atmos. Chem., 29, 109–118,
942 1998.
943 Latha, K. M., and Badarinath, K.: Seasonal variations of black carbon aerosols
944 and total aerosol mass concentrations over urban environment in India,
945 Atmos. Environ., 39, 4129–4141, 2005.
946 Lau, K. M., Kim, M. K., and Kim, K. M.: Asian summer monsoon anomalies
947 induced by aerosol direct forcing: the role of the Tibetan Plateau, Clim.
948 Dyn., 26, 855–864, doi:10.1007/s00382-006-0114-z, 2006.
949 Lawrence, M. G., and Lelieveld, J.: Atmospheric pollutant outflow from
950 southern Asia: a review, Atmos. Chem. Phys., 10, 11017-11096,
951 doi:10.5194/acp-10-11017-2010, 2010.
952 Lelieveld, J., Crutzen, P. J., Ramanathan, V., Andreae, M. O., Brenninkmeijer,
953 C. A. M., Campos, T., Cass, G. R., Dickerson, R. R., Fischer, H., de Gouw,
954 J. A., Hansel, A., Jefferson, A., Kley, D., de Laat, A. T. J., Lal, S., Lawrence,
955 M. G., Lobert, J. M., Mayol-Bracero, O. L., Mitra, A. P., Novakov, T.,
956 Oltmans, S. J., Prather, K. A., Reiner, T., Rodhe, H., Scheeren, H. A.,
957 Sikka, D., and Williams, J.: The Indian Ocean Experiment: Widespread air
958 pollution from South and Southeast Asia, Science, 291, 1031–1036,
959 doi:10.1126/science.1057103, 2001.
960 Leon, J.-F., Chazette, P., Dulac, F., Pelon, J., Flamant, C., Bonazzola, M.,
961 Foret, G., Alfaro, S., Cachier, H., and Cautenet, S.: Large-scale advection
962 of continental aerosols during INDOEX, J. Geophys. Res., 106,
963 28427–28428, 28439, 2001.
964 Li, Q., Jiang, J. H., Wu, D. L., Read, W. G., Livesey, N. J., Waters, J. W., Zhang,
965 Y., Wang, B., Filipiak, M. J., and Davis, C. P.: Convective outflow of South
966 Asian pollution: A global CTM simulation compared with EOS MLS
967 observations, Geophys. Res. Lett., 32, L14826,
968 doi:10.1029/2005GL022762, 2005.
969 Liao, H., Adams, P. J., Chung, S. H., Seinfeld, J. H., Mickley, L. J., and Jacob,
970 D. J.: Interactions between tropospheric chemistry and aerosols in a
971 unified general circulation model, J. Geophys. Res., 108, 4001,
972 doi:10.1029/2001JD001260, 2003.
973 Liao, H., and Seinfeld, J. H.: Global impacts of gas-phase chemistry-aerosol

974 interactions on direct radiative forcing by anthropogenic aerosols and
975 ozone, J. Geophys. Res., 110, D18208, doi:10.1029/2005JD005907,
976 2005.
977 Liao, H., Zhang, Y., Chen, W.-T., Raes, F., and Seinfeld, J. H.: Effect of
978 chemistry-aerosol-climate coupling on predictions of future climate and
979 future levels of tropospheric ozone and aerosols, J. Geophys. Res., 114,
980 D10306, doi:10.1029/2008JD010984, 2009.
981 Liu, H., Jacob, D. J., Bey, I., and Yantosca, R. M.: Constraints from 210Pb and
982 7Be on wet deposition and transport in a global three-dimensional
983 chemical tracer model driven by assimilated meteorological fields, J.
984 Geophys. Res., 106, 12109–12128, 2001.
985 Liu, X., Penner, J. E., and Wang, M.: Influence of anthropogenic sulfate and
986 black carbon on upper tropospheric clouds in the NCAR CAM3 model
987 coupled to the IMPACT global aerosol model, J. Geophys. Res., 114,
988 D03204, doi:10.1029/2008JD010492, 2009.
989 Livesey, N. J., Filipiak, M. J., Froidevaux, L., Read, W. G., Lambert, A., Santee,
990 M. L., Jiang, J. H., Pumphrey, H. C., Waters, J. W., and Cofield, R. E.:
991 Validation of Aura Microwave Limb Sounder O_3 and CO observations in
992 the upper troposphere and lower stratosphere, J. Geophys. Res., 113,
993 D15S02, doi:10.1029/2007JD008805, 2008.
994 Livesey, N. J., Read, W. G., Wagner, P. A., Froidevaux, L., Lambert, A.,
995 Manney, G. L., Pumphrey, H. C., Santee, M. L., Schwartz, M. J., Wang, S.,
996 Cofield, R. E., Cuddy, D. T., Fuller, R. A., Jarnot, R. F., Jiang, J. H., and
997 Knosp, B. W.: Version 3.3 Level 2 data quality and description document,
998 JPL D-33509, 2011.
999 Lodhi, A., Ghauri, B., Khan, M. R., Rahman, S., and Shafique, S.: Particulate
1000 matter ($PM_{2.5}$) concentration and source apportionment in Lahore, J.
1001 Brazil. Chem. Soc., 20, 1811–1820, 2009.
1002 Lou, S., Liao, H., and Zhu, B.: Impacts of aerosols on surface-layer ozone
1003 concentrations in China through heterogeneous reactions and changes in
1004 photolysis rates, Atmos. Environ., 85, 123–138, 2014.
1005 Ma, J., Tang, J., Li, S.-M., and Jacobson, M. Z.: Size distributions of ionic
1006 aerosols measured at Waliguan Observatory: Implication for nitrate
1007 gas-to-particle transfer processes in the free troposphere, J. Geophys.
1008 Res., 108, 4541, doi:10.1029/2002jd003356, 2003.
1009 Martin, R. V., Jacob, D. J., Yantosca, R. M., Chin, M., and Ginoux, P.: Global
1010 and regional decreases in tropospheric oxidants from photochemical
1011 effects of aerosols, J. Geophys. Res., 108, 4097,
1012 doi:10.1029/2002JD002622, 2003.
1013 McCormick, M. P.: SAGE II: an overview, Adv. Space Res., 7, 219-226, 1987.
1014 McLinden, C., Olsen, S., Hannegan, B., Wild, O., Prather, M., and Sundet, J.:
1015 Stratospheric ozone in 3-D models: A simple chemistry and the
1016 cross-tropopause flux, J. Geophys. Res., 105, 14653–14665,
1017 doi:10.1029/2000JD900124, 2000.
1018 Mickley, L. J., Murti, P., Jacob, D. J., Logan, J. A., Koch, D., and Rind, D.:
1019 Radiative forcing from tropospheric ozone calculated with a unified
1020 chemistry-climate model, J. Geophys. Res., 104, 30153-30172, 1999.
1021 Ming, J., Zhang, D., Kang, S., and Tian, W.: Aerosol and fresh snow chemistry
1022 in the East Rongbuk Glacier on the northern slope of Mt. Qomolangma
1023 (Everest), J. Geophys. Res., 112, D15307, doi:10.1029/2007JD008618,

2007.
Momin, G. A., Rao, P. S. P., Safai, P. D., Ali, K., Naik, M. S., and Pillai, A. G.: Atmospheric aerosol characteristic studies at Pune and Thiruvananthapuram during INDOEX programme–1998, Curr. Sci., 76, 985-989, 1999.
Mu, Q., and Liao, H.: Simulation of the interannual variations of aerosols in China: role of variations in meteorological parameters, Atmos. Chem. Phys., 14, 9597–9612, 2014.
Murray, L. T., Jacob, D. J., Logan, J. A., Hudman, R. C., and Koshak, W. J.: Optimized regional and interannual variability of lightning in a global chemical transport model constrained by LIS/OTD satellite data, J. Geophys. Res., 117, D20307, doi:10.1029/2012JD017934, 2012.
Nair, P. R., George, S. K., Sunilkumar, S., Parameswaran, K., Jacob, S., and Abraham, A.: Chemical composition of aerosols over peninsular India during winter, Atmos. Environ., 40, 6477–6493, 2006.
Nair, V. S., Solmon, F., Giorgi, F., Mariotti, L., Babu, S. S., and Moorthy, K. K.: Simulation of South Asian aerosols for regional climate studies, J. Geophys. Res., 117, D04209, doi:10.1029/2011JD016711, 2012.
Nakamura, T., Matsumoto, K., and Uematsu, M.: Chemical characteristics of aerosols transported from Asia to the East China Sea: an evaluation of anthropogenic combined nitrogen deposition in autumn, Atmos. Environ., 39, 1749–1758, 2005.
Oberbeck, V. R., Livingston, J. M., Russell, P. B., Pueschel, R. F., Rosen, J. N., Osborn, M. T., Kritz, M. A., Snetsinger, K. G., and Ferry, G. V.: SAGE II aerosol validation: Selected altitude measurements, including particle micromeasurements, J. Geophys. Res., 94, 8367–8380, doi:10.1029/JD094iD06p08367, 1989.
Pant, P., Hegde, P., Dumka, U., Sagar, R., Satheesh, S., Moorthy, K. K., Saha, A., and Srivastava, M.: Aerosol characteristics at a high-altitude location in central Himalayas: Optical properties and radiative forcing, J. Geophys. Res., 111, D17206, doi:10.1029/2005JD006768, 2006.
Park, M., Randel, W. J., Kinnison, D. E., Garcia, R. R., and Choi, W.: Seasonal variation of methane, water vapor, and nitrogen oxides near the tropopause: Satellite observations and model simulations, J. Geophys. Res., 109, D03302, doi:10.1029/2003JD003706, 2004.
Park, M., Randel, W. J., Gettelman, A., Massie, S. T., and Jiang, J. H.: Transport above the Asian summer monsoon anticyclone inferred from Aura Microwave Limb Sounder tracers, J. Geophys. Res., 112, D16309, doi:10.1029/2006JD008294, 2007.
Park, M., Randel, W. J., Emmons, L. K., Bernath, P. F., Walker, K. A., and Boone, C. D.: Chemical isolation in the Asian monsoon anticyclone observed in Atmospheric Chemistry Experiment (ACE–FTS) data, Atmos. Chem. Phys., 8, 757–764, 2008.
Park, M., Randel, W. J., Emmons, L. K., and Livesey, N. J.: Transport pathways of carbon monoxide in the Asian summer monsoon diagnosed from Model of Ozone and Related Tracers (MOZART), J. Geophys. Res., 114, D08303, doi:10.1029/2008JD010621, 2009.
Park, R. J., Jacob, D. J., Chin, M., and Martin, R. V.: Sources of carbonaceous aerosols over the United States and implications for natural visibility, J. Geophys. Res., 108, 4355, doi:10.1029/2002JD003190, 2003.

1074 Park, R. J., Jacob, D. J., Field, B. D., Yantosca, R. M., and Chin, M.: Natural
1075 and transboundary pollution influences on sulfate–nitrate–ammonium
1076 aerosols in the United States: Implications for policy, J. Geophys. Res.,
1077 109, D15204, doi:10.1029/2003JD004473, 2004.
1078 Pitari, G., Aquila, V., Kravitz, B., Robock, A., Watanabe, S., Cionni, I., Luca, N.
1079 D., Genova, G. D., Mancini, E., and Tilmes, S.: Stratospheric ozone
1080 response to sulfate geoengineering: Results from the Geoengineering
1081 Model Intercomparison Project (GeoMIP), J. Geophys. Res., 119,
1082 2629–2653, doi: 10.1002/2013JD020566, 2014.
1083 Popp, P., Marcy, T., Jensen, E., Kärcher, B., Fahey, D., Gao, R., Thompson, T.,
1084 Rosenlof, K., Richard, E., and Herman, R.: The observation of nitric
1085 acid-containing particles in the tropical lower stratosphere, Atmos. Chem.
1086 Phys., 6, 601-611, 2006.
1087 Pye, H., Liao, H., Wu, S., Mickley, L. J., Jacob, D. J., Henze, D. K., and
1088 Seinfeld, J.: Effect of changes in climate and emissions on future
1089 sulfate–nitrate–ammonium aerosol levels in the United States, J. Geophys.
1090 Res., 114, D01205, doi:10.1029/2008JD010701, 2009.
1091 Qie, X., Wu, X., Yuan, T., Bian, J., and Lü, D.: Comprehensive Pattern of Deep
1092 Convective Systems over the Tibetan Plateau–South Asian Monsoon
1093 Region Based on TRMM Data, J. Clim., 27, 6612–6626, 2014.
1094 Ram, K., Sarin, M., and Hegde, P.: Atmospheric abundances of primary and
1095 secondary carbonaceous species at two high-altitude sites in India:
1096 Sources and temporal variability, Atmos. Environ., 42, 6785-6796, 2008.
1097 Ramanathan, V., Li, F., Ramana, M., Praveen, P., Kim, D., Corrigan, C.,
1098 Nguyen, H., Stone, E. A., Schauer, J. J., and Carmichael, G.: Atmospheric
1099 brown clouds: Hemispherical and regional variations in long-range
1100 transport, absorption, and radiative forcing, J. Geophys. Res., 112,
1101 D22S21, doi:10.1029/2006JD008124, 2007.
1102 Randel, W. J., and Park, M.: Deep convective influence on the Asian summer
1103 monsoon anticyclone and associated tracer variability observed with
1104 Atmospheric Infrared Sounder (AIRS), J. Geophys. Res., 111, D12314,
1105 doi:10.1029/2005JD006490, 2006.
1106 Randel, W. J., Park, M., Emmons, L., Kinnison, D., Bernath, P., Walker, K. A.,
1107 Boone, C., and Pumphrey, H.: Asian monsoon transport of pollution to the
1108 stratosphere, Science, 328, 611–613, 2010.
1109 Rasch, P. J., Tilmes, S., Turco, R. P., Robock, A., Oman, L., Chen, C. C.,
1110 Stenchikov, G. L., and Garcia, R. R.: An overview of geoengineering of
1111 climate using stratospheric sulphate aerosols, Philos. Trans. R. Soc.
1112 A-Math. Phys. Eng. Sci., 366, 4007-4037, doi:10.1098/rsta.2008.0131,
1113 2008.
1114 Rastogi, N., and Sarin, M.: Long-term characterization of ionic species in
1115 aerosols from urban and high-altitude sites in western India: Role of
1116 mineral dust and anthropogenic sources, Atmos. Environ., 39, 5541–5554,
1117 2005.
1118 Rastogi, N., and Sarin, M.: Quantitative chemical composition and
1119 characteristics of aerosols over western India: one-year record of
1120 temporal variability, Atmos. Environ., 43, 3481–3488, 2009.
1121 Rengarajan, R., Sarin, M., and Sudheer, A.: Carbonaceous and inorganic
1122 species in atmospheric aerosols during wintertime over urban and
1123 high-altitude sites in North India, J. Geophys. Res., 112, D21307,

1124 doi:10.1029/2006JD008150, 2007.
1125 Russell, P. B., and Mccormick, M. P.: SAGE II aerosol data validation and initial
1126 data use: An introduction and overview, J. Geophys. Res., 94, 8335–8338,
1127 1989.
1128 Safai, P., Kewat, S., Praveen, P., Rao, P., Momin, G., Ali, K., and Devara, P.:
1129 Seasonal variation of black carbon aerosols over a tropical urban city of
1130 Pune, India, Atmos. Environ., 41, 2699–2709, 2007.
1131 Salam, A., Bauer, H., Kassin, K., Mohammad Ullah, S., and Puxbaum, H.:
1132 Aerosol chemical characteristics of a mega-city in Southeast Asia
1133 (Dhaka–Bangladesh), Atmos. Environ., 37, 2517–2528, 2003.
1134 Santee, M., Lambert, A., Read, W., Livesey, N., Cofield, R., Cuddy, D., Daffer,
1135 W., Drouin, B., Froidevaux, L., and Fuller, R.: Validation of the Aura
1136 Microwave Limb Sounder HNO_3 measurements, J. Geophys. Res., 112,
1137 D24S40, doi:10.1029/2007JD008721, 2007.
1138 Sauvage, B., Martin, R., Donkelaar, A. v., Liu, X., Chance, K., Jaeglé, L.,
1139 Palmer, P., Wu, S., and Fu, T.-M.: Remote sensed and in situ constraints
1140 on processes affecting tropical tropospheric ozone, Atmos. Chem. Phys.,
1141 7, 815–838, 2007.
1142 Seinfeld, J. H., and Pandis, S. N.: Atmospheric chemistry and physics: from air
1143 pollution to climate change, Environment Science & Policy for Sustainable
1144 Development, 51, 212–214(213), 2006.
1145 Sharma, R. K., Bhattarai, B., Sapkota, B., Gewali, M., and Kjeldstad, B.: Black
1146 carbon aerosols variation in Kathmandu valley, Nepal, Atmos. Environ., 63,
1147 282–288, doi:10.1016/j.atmosenv.2012.09.023, 2012.
1148 Shrestha, A. B., Wake, C. P., Dibb, J. E., Mayewski, P. A., Whitlow, S. I.,
1149 Carmichael, G. R., and Ferm, M.: Seasonal variations in aerosol
1150 concentrations and compositions in the Nepal Himalaya, Atmos. Environ.,
1151 34, 3349–3363, 10.1016/s1352-2310(99)00366-0, 2000.
1152 Š kerlak, B., Sprenger, M., and Wernli, H.: A global climatology of
1153 stratosphere-troposphere exchange using the ERA-Interim data set from
1154 1979 to 2011, Atmos. Chem. Phys, 14, 913–937, 2014.
1155 Stevenson, D. S., Dentener, F. J., Schultz, M. G., Ellingsen, K., Van Noije, T. P.
1156 C., Wild, O., Zeng, G., Amann, M., Atherton, C. S., and Bell, N.:
1157 Multimodel ensemble simulations of present-day and near-future
1158 tropospheric ozone, J. Geophys. Res., 111, D08301,
1159 doi:10.1029/2005JD006338, 2006.
1160 Streets, D. G., Bond, T. C., Carmichael, G. R., Fernandes, S. D., Fu, Q., He, D.,
1161 Klimont, Z., Nelson, S. M., Tsai, N. Y., and Wang, M. Q.: An inventory of
1162 gaseous and primary aerosol emissions in Asia in the year 2000, J.
1163 Geophys. Res., 108, GTE 30–31, 2003.
1164 Su, H., Jiang, J. H., Lu, X. H., Penner, J. E., Read, W. G., Massie, S.,
1165 Schoeberl, M. R., Colarco, P., Livesey, N. J., and Santee, M. L.: Observed
1166 Increase of TTL Temperature and Water Vapor in Polluted Clouds over
1167 Asia, J. Clim., 24, 2728–2736, 10.1175/2010jcli3749.1, 2011.
1168 Sudheer, A., and Sarin, M.: Carbonaceous aerosols in MABL of Bay of Bengal:
1169 Influence of continental outflow, Atmos. Environ., 42, 4089-4100, 2008.
1170 Talukdar, R. K., Burkholder, J. B., Roberts, J. M., Portmann, R. W., and
1171 Ravishankara, A.: Heterogeneous Interaction of N_2O_5 with HCl Doped
1172 H_2SO_4 under Stratospheric Conditions: $ClNO_2$ and Cl_2 Yields, J. Phys.
1173 Chem. A., 116, 6003–6014, 2012.

1174 Tang, M., Telford, P., Pope, F., Rkiouak, L., Abraham, N., Archibald, A.,
1175 Braesicke, P., Pyle, J., McGregor, J., and Watson, I.: Heterogeneous
1176 reaction of N_2O_5 with airborne TiO_2 particles and its implication for
1177 stratospheric particle injection, Atmos. Chem. Phys., 14, 6035–6048,
1178 2014.
1179 Tare, V., Tripathi, S., Chinnam, N., Srivastava, A., Dey, S., Manar, M.,
1180 Kanawade, V. P., Agarwal, A., Kishore, S., and Lal, R.: Measurements of
1181 atmospheric parameters during Indian Space Research Organization
1182 Geosphere Biosphere Program Land Campaign II at a typical location in
1183 the Ganga Basin: 2. chemical properties, J. Geophys. Res., 111, D23210,
1184 doi:10.1029/2006JD007279, 2006.
1185 Thornton, J. A., Jaeglé, L., and McNeill, V. F.: Assessing known pathways for
1186 HO_2 loss in aqueous atmospheric aerosols: Regional and global impacts
1187 on tropospheric oxidants, J. Geophys. Res., 113, D05303,
1188 doi:10.1029/2007JD009236, 2008.
1189 Tobo, Y., Zhang, D., Iwasaka, Y., and Shi, G.: On the mixture of aerosols and
1190 ice clouds over the Tibetan Plateau: Results of a balloon flight in the
1191 summer of 1999, Geophys. Res. Lett., 34, L23801,
1192 doi:10.1029/2007GL031132, 2007.
1193 Tripathi, S., Dey, S., Tare, V., and Satheesh, S.: Aerosol black carbon radiative
1194 forcing at an industrial city in northern India, Geophys. Res. Lett., 32,
1195 L08802, doi:10.1029/2005GL022515, 2005.
1196 van der Werf, G. R., Randerson, J. T., Giglio, L., Collatz, G. J., Mu, M.,
1197 Kasibhatla, P. S., Morton, D. C., DeFries, R. S., Jin, Y., and van Leeuwen,
1198 T. T.: Global fire emissions and the contribution of deforestation, savanna,
1199 forest, agricultural, and peat fires (1997–2009), Atmos. Chem. Phys., 10,
1200 11707–11735, 2010.
1201 Vanhellemont, F., Tetard, C., Bourassa, A., Fromm, M., Dodion, J., Fussen, D.,
1202 Brogniez, C., Degenstein, D., Gilbert, K., and Turnbull, D.: Aerosol
1203 extinction profiles at 525 nm and 1020 nm derived from ACE imager data:
1204 comparisons with GOMOS, SAGE II, SAGE III, POAM III, and OSIRIS,
1205 Atmos. Chem. Phys., 8, 2027-2037, 2008.
1206 Venkataraman, C., Reddy, C. K., Josson, S., and Reddy, M. S.: Aerosol size
1207 and chemical characteristics at Mumbai, India, during the INDOEX-IFP
1208 (1999), Atmos. Environ., 36, 1979–1991, 2002.
1209 Verma, S., Boucher, O., Reddy, M., Upadhyaya, H., Van, P., Binkowski, F., and
1210 Sharma, O.: Tropospheric distribution of sulphate aerosols mass and
1211 number concentration during INDOEX-IFP and its transport over the
1212 Indian Ocean: a GCM study, Atmos. Chem. Phys., 12, 6185–6196, 2012.
1213 Vernier, J.-P., Pommereau, J.-P., Garnier, A., Pelon, J., Larsen, N., Nielsen, J.,
1214 Christensen, T., Cairo, F., Thomason, L., and Leblanc, T.: Tropical
1215 stratospheric aerosol layer from CALIPSO lidar observations, J. Geophys.
1216 Res., 114, D00H10, doi:10.1029/2009JD011946, 2009.
1217 Vernier, J. P., Thomason, L., and Kar, J.: CALIPSO detection of an Asian
1218 tropopause aerosol layer, Geophys. Res. Lett., 38, L07804,
1219 doi:10.1029/2010GL046614, 2011.
1220 Voigt, C., Schreiner, J., Kohlmann, A., Zink, P., Mauersberger, K., Larsen, N.,
1221 Deshler, T., Kröger, C., Rosen, J., and Adriani, A.: Nitric acid trihydrate
1222 (NAT) in polar stratospheric clouds, Science, 290, 1756-1758, 2000.
1223 Wang, P., McCormick, M., McMaster, L., Chu, W., Swissler, T., Osborn, M.,

Russell, P., Oberbeck, V., Livingston, J., and Rosen, J.: SAGE II aerosol data validation based on retrieved aerosol model size distribution from SAGE II aerosol measurements, J. Geophys. Res., 94, 8381–8393, doi:10.1029/JD094iD06p08381, 1989.

Wang, Y., Logan, J. A., and Jacob, D. J.: Global simulation of tropospheric O_3–NO_x–hydrocarbon chemistry: 2. Model evaluation and global ozone budget, J. Geophys. Res., 103, 10727–10755, 1998.

Wang, Y., Zhang, Q., He, K., Zhang, Q., and Chai, L.: Sulfate-nitrate-ammonium aerosols over China: response to 2000–2015 emission changes of sulfur dioxide, nitrogen oxides, and ammonia, Atmos. Chem. Phys., 13, 2635–2652, 2013.

Waters, J. W., Froidevaux, L., Harwood, R. S., Jarnot, R. F., Pickett, H. M., Read, W. G., Siegel, P. H., Cofield, R. E., Filipiak, M. J., and Flower, D.: The earth observing system microwave limb sounder (EOS MLS) on the Aura satellite, IEEE T. Geosci. Remote., 44, 1075-1092, 2006.

Weigel, R., Borrmann, S., Kazil, J., Minikin, A., Stohl, A., Wilson, J., Reeves, J., Kunkel, D., De Reus, M., and Frey, W.: In situ observations of new particle formation in the tropical upper troposphere: the role of clouds and the nucleation mechanism, Atmos. Chem. Phys. Discuss., 11, 2011.

Wesely, M.: Parameterization of surface resistances to gaseous dry deposition in regional-scale numerical models, Atmos. Environ., 23, 1293-1304, 1989.

Wu, L. T., Su, H., and Jiang, J. H.: Regional simulations of deep convection and biomass burning over South America: 2. Biomass burning aerosol effects on clouds and precipitation, J. Geophys. Res., 116, doi:10.1029/2011jd01 6106, 2011.

Wu, S., Mickley, L. J., Jacob, D. J., Logan, J. A., Yantosca, R. M., and Rind, D.: Why are there large differences between models in global budgets of tropospheric ozone? J. Geophys. Res., 112, D05302, doi:10.1029/2006JD007801, 2007.

Wu, S., Mickley, L. J., Jacob, D. J., Rind, D., and Streets, D. G.: Effects of 2000–2050 changes in climate and emissions on global tropospheric ozone and the policy–relevant background surface ozone in the United States, J. Geophys. Res., 113, D18312, doi:10.1029/2007JD009639, 2008.

Xia, X., Zong, X., Cong, Z., Chen, H., Kang, S., and Wang, P.: Baseline continental aerosol over the central Tibetan plateau and a case study of aerosol transport from South Asia, Atmos. Environ., 45, 7370-7378, 2011.

Xiong, X., Houweling, S., Wei, J., Maddy, E., Sun, F., and Barnet, C.: Methane plume over south Asia during the monsoon season: satellite observation and model simulation, Atmos. Chem. Phys., 9, 783-794, 2009.

Yanai, M., Li, C., and Song, Z.: Seasonal heating of the Tibetan Plateau and its effects on the evolution of the Asian summer monsoon, J. Meteorol. Soc. Jan., 70, 319–351, 1992.

Yao, X., Chan, C. K., Fang, M., Cadle, S., Chan, T., Mulawa, P., He, K., and Ye, B.: The water-soluble ionic composition of $PM_{2.5}$ in Shanghai and Beijing, China, Atmos. Environ., 36, 4223–4234, 2002.

Yin, Y., Chen, Q., Jin, L., Chen, B., Zhu, S., and Zhang, X.: The effects of deep convection on the concentration and size distribution of aerosol particles within the upper troposphere: A case study, J. Geophys. Res., 117,

1274 D22202, doi:10.1029/2012JD017827, 2012.
1275 Zeng, G., Pyle, J., and Young, P.: Impact of climate change on tropospheric
1276 ozone and its global budgets, Atmos. Chem. Phys., 8, 369-387, 2008.
1277 Zhang, G. J., and McFarlane, N. A.: Sensitivity of climate simulations to the
1278 parameterization of cumulus convection in the Canadian Climate Centre
1279 general circulation model, Atmos.-Ocean, 33, 407–446, 1995.
1280 Zhang, L., Liao, H., and Li, J.: Impacts of Asian summer monsoon on seasonal
1281 and interannual variations of aerosols over eastern China, J. Geophys.
1282 Res., 115, D00K05, doi:10.1029/2009JD012299, 2010.
1283 Zhang, N., Cao, J., Ho, K., and He, Y.: Chemical characterization of aerosol
1284 collected at Mt. Yulong in wintertime on the southeastern Tibetan Plateau,
1285 Atmos. Res., 107, 76, 2012.
1286 Zhang, Q., Streets, D. G., Carmichael, G. R., He, K., Huo, H., Kannari, A.,
1287 Klimont, Z., Park, I., Reddy, S., and Fu, J.: Asian emissions in 2006 for the
1288 NASA INTEX-B mission, Atmos. Chem. Phys., 9, 5131–5153, 2009.
1289 Zhang, X., Cao, J., Li, L., Arimoto, R., Cheng, Y., Huebert, B., and Wang, D.:
1290 Characterization of atmospheric aerosol over Xian in the south margin of
1291 the Loess Plateau, China, Atmos. Environ., 36, 4189–4199, 2002.
1292 Zhang, X. Y., Wang, Y. Q., Niu, T., Zhang, X. C., Gong, S. L., Zhang, Y. M., and
1293 Sun, J. Y.: Atmospheric aerosol compositions in China: spatial/temporal
1294 variability, chemical signature, regional haze distribution and comparisons
1295 with global aerosols, Atmos. Chem. Phys., 12, 779–799,
1296 doi:10.5194/acp-12-779-2012, 2012.
1297 Zhang, Y., Dore, A., Ma, L., Liu, X., Ma, W., Cape, J., and Zhang, F.:
1298 Agricultural ammonia emissions inventory and spatial distribution in the
1299 North China Plain, Environ. Pollut., 158, 490–501, 2010.
1300 Zhao, X., Turco, R. P., Kao, C. Y. J., and Elliott, S.: Aerosol-induced chemical
1301 perturbations of stratospheric ozone: Three-dimensional simulations and
1302 analysis of mechanisms, J. Geophys. Res., 102, 3617–3637,
1303 doi:10.1029/96jd03406, 1997.
1304 Zhu, J., Liao, H., and Li, J.: Increases in aerosol concentrations over
1305 eastern China due to the decadal-scale weakening of the East Asian
1306 summer monsoon, Geophys. Res. Lett., 39, L09809,
1307 doi:10.1029/2012GL051428, 2012.

Table 1. Summary of Annual Emissions of Aerosols and Aerosol Precursors in Asia (60°E-155°E, 10°N-55°N)

Species	Global	Asia
NO_x (Tg N yr^{-1})		
Aircraft	0.5	0.08
Anthropogenic	28.6	9.96
Biomass burning	4.7	0.27
Fertilizer	0.7	0.31
Lightning	5.9	0.87
Soil	5.9	0.96
Total	46.3	12.45
SO_2 (Tg S yr^{-1})		
Aircraft	0.1	0.01
Anthropogenic	52.6	23.46
Biomass burning	1.2	0.07
Volcanoes	4.4	1.04
No_eruption	8.9	1.78
Ship	7.4	0.94
Total	74.6	27.30
NH_3 (Tg N yr^{-1})		
Anthropogenic	34.9	17.83
Natural	14.2	2.01
Biomass burning	3.5	0.21
Biofuel	1.6	0.71
Total	54.2	20.76
OC (Tg C yr^{-1})		
Anthropogenic	3.1	1.42
Biomass burning	18.7	1.10
Biofuel	6.3	3.28
Biogenic	9.7	1.22
Total	37.8	7.02
BC (Tg C yr^{-1})		
Anthropogenic	3.0	1.43
Biomass burning	2.2	0.12
Biofuel	1.6	0.86
Total	6.8	2.41

Table 2. Simulated seasonal mean concentrations of aerosols and their contributions to $PM_{2.5}$ (in percentages in parentheses) during summertime (June-August) of 2005 for the TP/SASM, TP, and SASM regions. The unit is μg m^{-3} for concentrations at the surface, and 10^{-2} μg m^{-3} for concentrations at 200 hPa and 100 hPa.

	$PM_{2.5}$	SO_4^{2-}	NO_3^-	NH_4^+	OC	BC
			TP/SASM			
Surface	4.73	1.70(35.9%)	0.94(19.8%)	0.85(18.1%)	0.94(19.8%)	0.30(6.4%)
200 hPa	16.19	3.27(20.2%)	7.57(46.8%)	2.67(16.5%)	2.22(13.7%)	0.44(2.7%)
100 hPa	12.14	2.60(21.4%)	6.90(56.8%)	1.43(11.8%)	1.05(8.6%)	0.16(1.3%)
			TP			
Surface	5.44	2.12(39.0%)	1.05(19.3%)	1.08(19.9%)	0.88(16.1%)	0.31(5.7%)
200 hPa	19.80	4.16(21.0%)	9.43(47.6%)	3.25(16.4%)	2.49(12.6%)	0.47(2.4%)
100 hPa	10.58	2.60(24.6%)	5.51(52.0%)	1.35(12.7%)	0.99(9.4%)	0.14(1.3%)
			SASM			
Surface	4.02	1.28(31.8%)	0.83(20.5%)	0.63(15.6%)	1.00(24.8%)	0.29(7.2%)
200 hPa	12.57	2.38(18.9%)	5.72(45.5%)	2.10(16.7%)	1.95(15.5%)	0.41(3.3%)
100 hPa	13.71	2.60(19.0%)	8.30(60.5%)	1.52(11.1%)	1.11(8.1%)	0.18(1.3%)

Table 3. Sensitivity simulations to examine the impacts of uncertainties in surface-layer aerosol concentrations on simulated NO_3^- in the UTLS. "Conc" and "Ctri" denote, respectively, simulated seasonal mean concentrations of SO_4^{2-}, NO_3^-, NH_4^+, OC, BC and their contributions to $PM_{2.5}$ (in percentages) during summertime (June-August) of 2005. The mass concentrations are averaged over the TP/SASM region, with unit of μg m^{-3} at the surface layer and of 10^{-2} μg m^{-3} at 200 hPa and 100 hPa. Also shown are the NMBs, as the simulated surface-layer concentrations are compared with measurements described in Section 4.2.

Species	Baseline Case			SO_2 (+20%)			NO_x (-50%)			NH_3 (-50%)			All Change		
	Conc.	Ctri.	NMB	Conc.	Ctri.	NMB	Conc.	Ctri.	NMB	Conc.	Ctri.	NMB	Conc.	Ctri.	NMB
Surface															
SO_4^{2-}	1.70	35.9%	–14.7%	1.92	38.1%	–4.4%	1.58	39.5%	–18.1%	1.70	38.1%	–14.7%	1.78	43.2%	–8.3%
NO_3^-	0.94	19.8%	+51.5%	0.94	18.7%	+53.5%	0.50	12.5%	–11.7%	0.73	16.4%	+24.1%	0.39	9.5%	–27.0%
NH_4^+	0.85	18.1%	+74.9%	0.94	18.6%	+93.8%	0.68	17.1%	+44.1%	0.78	17.6%	+64.6%	0.71	17.3%	+55.4%
OC	0.94	19.8%	–57.2%	0.94	18.6%	–57.2%	0.94	23.4%	–57.2%	0.94	21.0%	–57.2%	0.94	22.7%	–57.2%
BC	0.30	6.4%	–32.2%	0.30	6.0%	–32.2%	0.30	7.5%	–32.2%	0.30	6.8%	–32.2%	0.30	7.3%	–32.2%
200 hPa															
SO_4^{2-}	3.27	20.2%		3.67	22.9%		3.31	20.6%		3.29	29.1%		3.74	33.7%	
NO_3^-	7.57	46.8%		7.05	43.9%		7.41	46.0%		3.86	34.2%		3.19	28.7%	
NH_4^+	2.67	16.5%		2.67	16.6%		2.71	16.8%		1.49	13.2%		1.50	13.5%	
OC	2.22	13.7%		2.22	13.8%		2.22	13.8%		2.22	19.7%		2.22	20.0%	
BC	0.44	2.7%		0.44	2.7%		0.44	2.7%		0.44	3.9%		0.44	4.0%	
100 hPa															
SO_4^{2-}	2.60	21.4%		2.80	23.0%		2.66	21.9%		2.60	25.2%		2.87	27.2%	
NO_3^-	6.90	56.8%		6.72	55.3%		6.81	56.1%		5.68	55.0%		5.62	53.3%	
NH_4^+	1.43	11.8%		1.43	11.7%		1.45	12.0%		0.84	8.1%		0.84	8.0%	
OC	1.05	8.6%		1.05	8.6%		1.05	8.7%		1.05	10.2%		1.05	10.0%	
BC	0.16	1.3%		0.16	1.3%		0.16	1.3%		0.16	1.6%		0.16	1.5%	

Figure Captions

Figure. 1. Regions examined in this study: the Tibetan Plateau region (TP, 70–105°E, 25–40°N), the SASM region (SASM, 70–105°E, 10–25°N), and the anticyclone region of (20–120°E, 10–40°N).

Figure. 2. Monthly variations in emissions of NO_x (Tg N month^{-1}), SO_2 (Tg S month^{-1}), NH_3 (Tg N month^{-1}), OC (Tg C month^{-1}), and BC (Tg C month^{-1}) over Asia. Values shown are the total emissions (anthropogenic plus natural emissions listed in Table 1).

Figure. 3. Simulated global distributions of surface-layer HNO_3 (pptv) and O_3 (ppbv) averaged over June-August, 2005.

Figure. 4. Comparisons of simulated HNO_3 concentrations (pptv) with observations (pptv) from MLS. (a) and (b) are simulated concentrations at 200 hPa and 100 hPa, respectively. (c) is the latitude-altitude cross section of simulated HNO_3 concentrations averaged over 70–105°E. (d)-(f) are the same as (a)-(c), except that (d)-(f) are observations from MLS. The white areas in (d) and (f) have no datasets available from MLS. All the datasets are averaged over June-August of 2005.

Figure. 5. Comparisons of simulated O_3 concentrations (ppbv) with observations (ppbv) from MLS. (a) and (b) are simulated concentrations at 200 hPa and 100 hPa, respectively. (c) is the latitude-altitude cross section of simulated O_3 concentrations averaged over 70–105°E. (d)-(f) are the same as (a)-(c), except that (d)-(f) are observations from MLS. All the datasets are averaged over June-August of 2005.

Figure. 6. The simulated and observed vertical profiles of monthly mean O_3 mixing ratios at (a) Kunming and (b) Lhasa in August. The model results are from the simulation of year 2005. The observations in Kunming were conducted during August 7–13 (11 profiles of O_3 collected) in 2009 and during August 12–31 in 2012 (daily observations). The observations in Lhasa were conducted during August 22–28 in 2010 (12 profiles of O_3 collected) and during August 4–26 in 2013 (daily observations).

Figure. 7. Simulated seasonal mean concentrations (μg m^{-3}) of sulfate, nitrate, ammonium, organic carbon, black carbon, and $PM_{2.5}$ at (a) the surface layer, (b) 200 hPa, and (c) 100 hPa, during summer (June-August) of year 2005. Note that color bars are different for concentrations at the surface, 200 hPa, and 100 hPa.

Figure. 8. (a) Locations with measured aerosol concentrations from previous studies. Also shown are surface winds during summertime. (b)–(f) show the comparisons of simulated seasonal mean concentrations of sulfate, nitrate, ammonium, OC, and BC with measured values, respectively. Also shown in (b)–(f) are the 1:1 line (dashed), linear fit (solid line and equation), correlation coefficient between simulated and measured concentrations (R), and

normalized mean bias (NMB) (defined as NMB=$\frac{\sum_{i=1}^{n}(P_i-O_i)}{\sum_{i=1}^{n}O_i}$ ×100%, where P_i and O_i are predicted and observed concentrations at station *i* for each aerosol species).

Figure. 9. (a) Monthly mean distribution of aerosol extinction coefficients (km^{-1}) at 100 hPa for July of 2005. (b) Monthly mean vertical distributions of aerosol extinction coefficients (at 525 nm for SAGE II and 550 nm for GEOS-Chem) (km^{-1}) averaged over the Asian monsoon anticyclone region (20–120°E, 10–40°N) for July of 2005. The horizontal dashed line represents the tropopause averaged over the Asian monsoon anticyclone region simulated by the GEOS-Chem model.

Figure. 10. Simulated contributions of nitrate to $PM_{2.5}$ (C_{NIT}= [NIT]/ [$PM_{2.5}$] ×100%) averaged over summer (June-August) of year 2005 at (a) surface-layer, (b) 200 hPa, and (c) 100 hPa. (d) The latitude-altitude cross section of simulated C_{NIT} (%) averaged over 70–105°E.

Figure. 11. Latitude-altitude cross sections of simulated concentrations (color shades, μg m^{-3}) of SO_4^{2-} and NO_3^- averaged over 70–105°E in June-August of 2005, together with the wind vectors obtained from the European Centre for Medium-Range Weather Forecasts (ECMWF) ERA-Interim Reanalysis data. The black line is the tropopause simulated by the GEOS-Chem model.

Figure. 12. (a)-(b) Distributions of RH (%) and temperature (K) at 100 hPa. (c)-(d) The latitude-altitude cross sections of RH (%) and temperature (K) averaged over 70–105°E. RH and temperature are from the GEOS5 assimilated meteorological fields, and all the values are the averages over June-August of year 2005.

Figure. 13. Mass budget for nitrate aerosol within the selected box of (70–105°E, 10–40°N, 8–16 km). E/W transport indicates net mass flux through the east and west lateral boundaries, N/S transport indicates net mass flux through the north and south lateral boundaries, and upward transport is the net mass flux through the top and bottom sides of the box. The mass flux is positive if it increases nitrate mass within the box. Unit of fluxes is Tg $season^{-1}$. All the values are the averages over June-August of 2005.

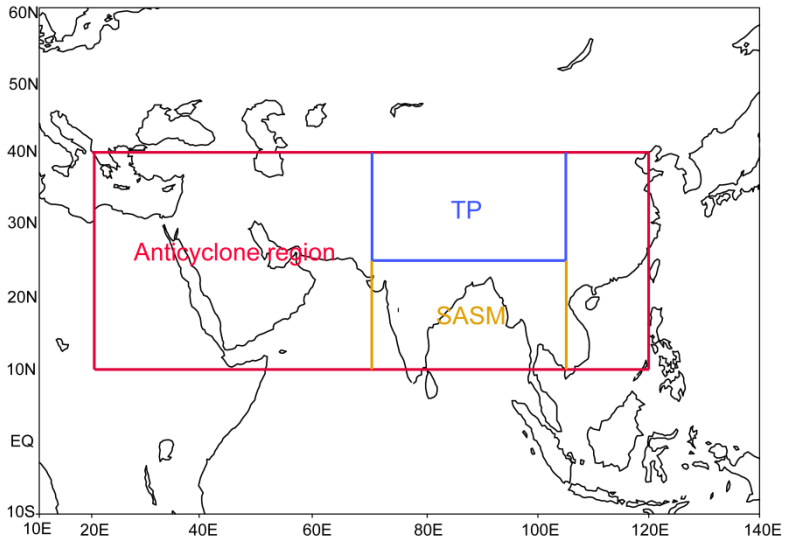

Figure. 1. Regions examined in this study: the Tibetan Plateau region (TP, 70–105°E, 25–40°N), the SASM region (SASM, 70–105°E, 10–25°N), and the anticyclone region of (20–120°E, 10–40°N).

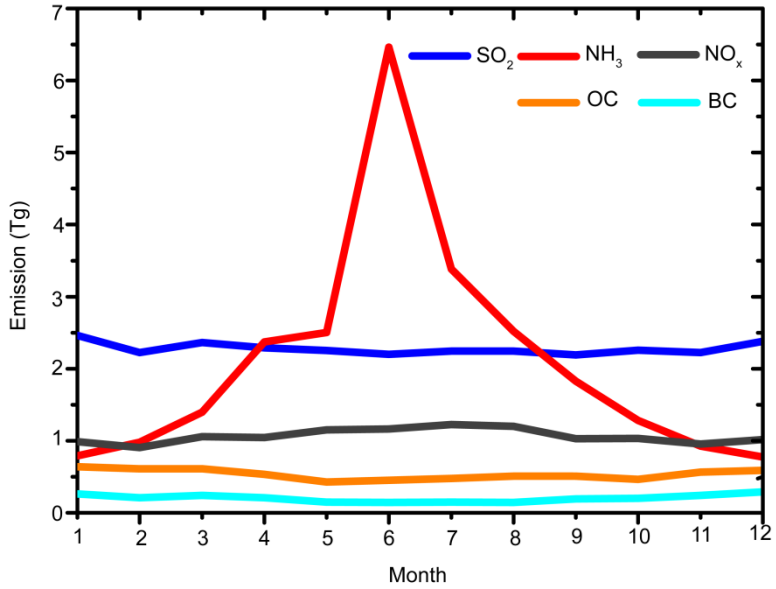

Figure. 2. Monthly variations in emissions of NO_x (Tg N month $^{-1}$), SO_2 (Tg S month^{-1}), NH_3 (Tg N month $^{-1}$), OC (Tg C month $^{-1}$), and BC (Tg C month $^{-1}$) over Asia. Values shown are the total emissions (anthropogenic plus natural emissions listed in Table 1).

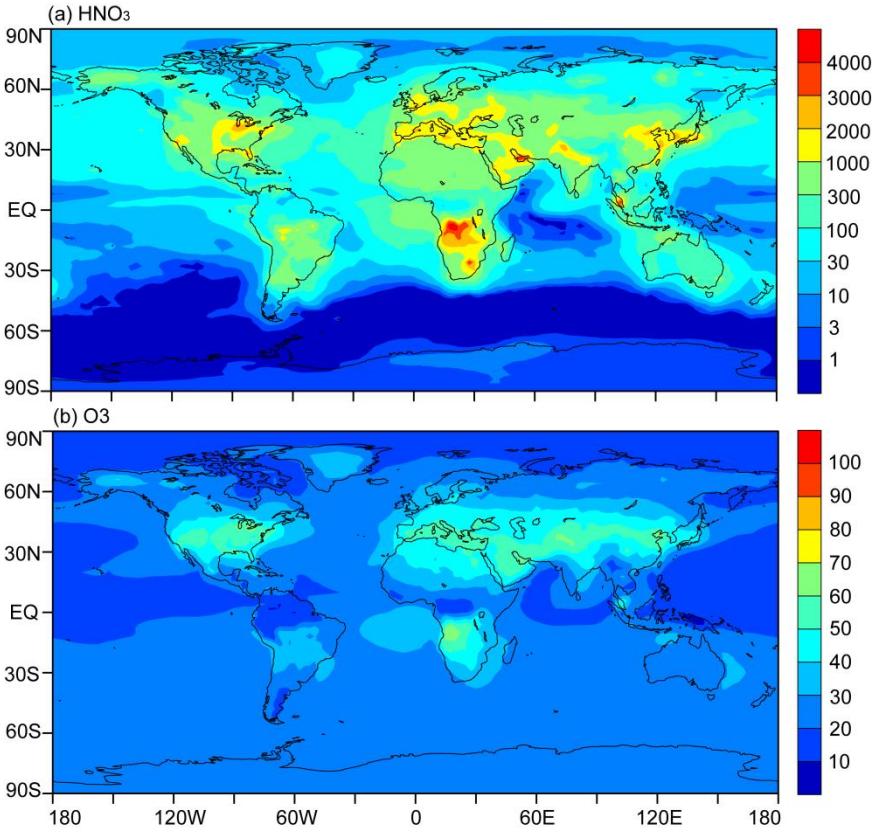

Figure. 3. Simulated global distributions of surface-layer HNO_3 (pptv) and O_3 (ppbv) averaged over June-August, 2005.

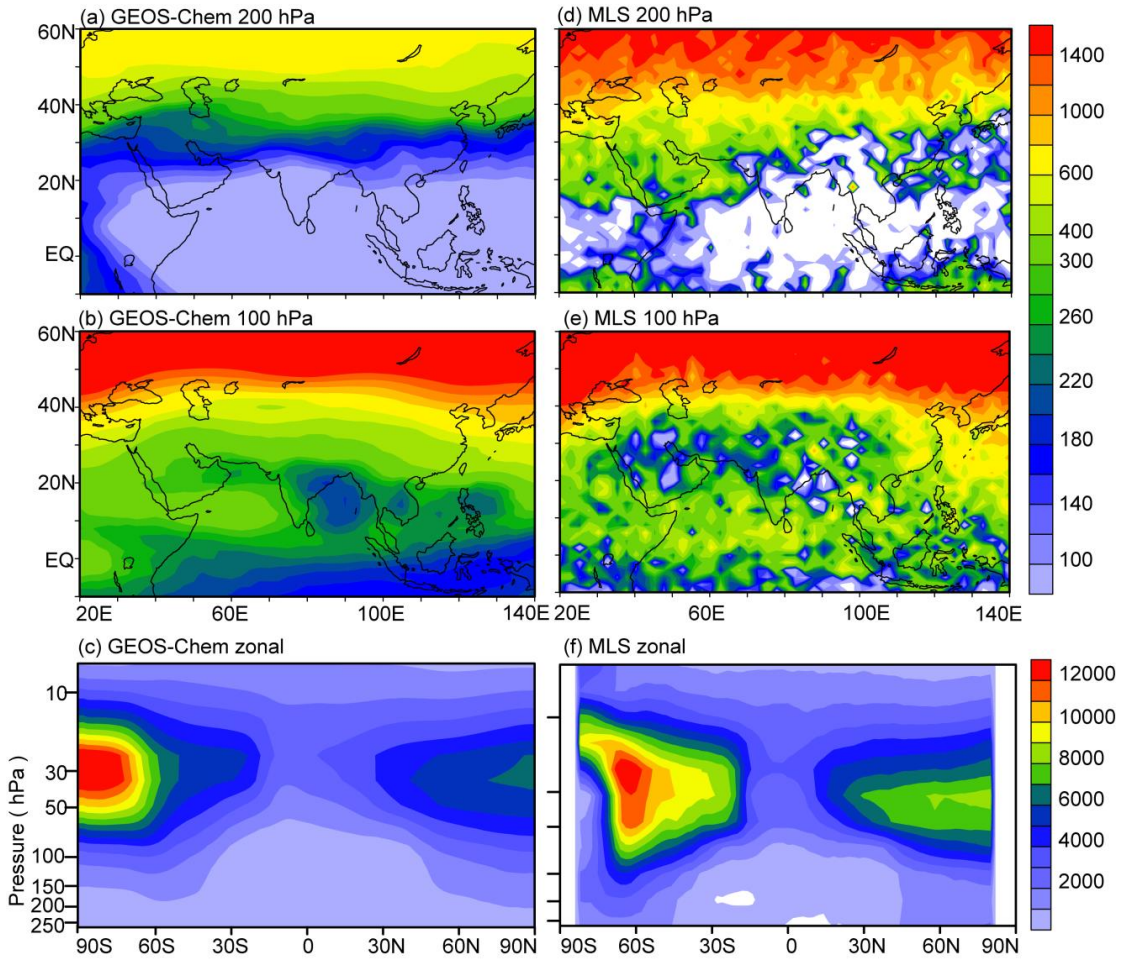

Figure. 4. Comparisons of simulated HNO_3 concentrations (pptv) with observations (pptv) from MLS. (a) and (b) are simulated concentrations at 200 hPa and 100 hPa, respectively. (c) is the latitude-altitude cross section of simulated HNO_3 concentrations averaged over 70–105°E. (d)-(f) are the same as (a)-(c), except that (d)-(f) are observations from MLS. The white areas in (d) and (f) have no datasets available from MLS. All the datasets are averaged over June-August of 2005.

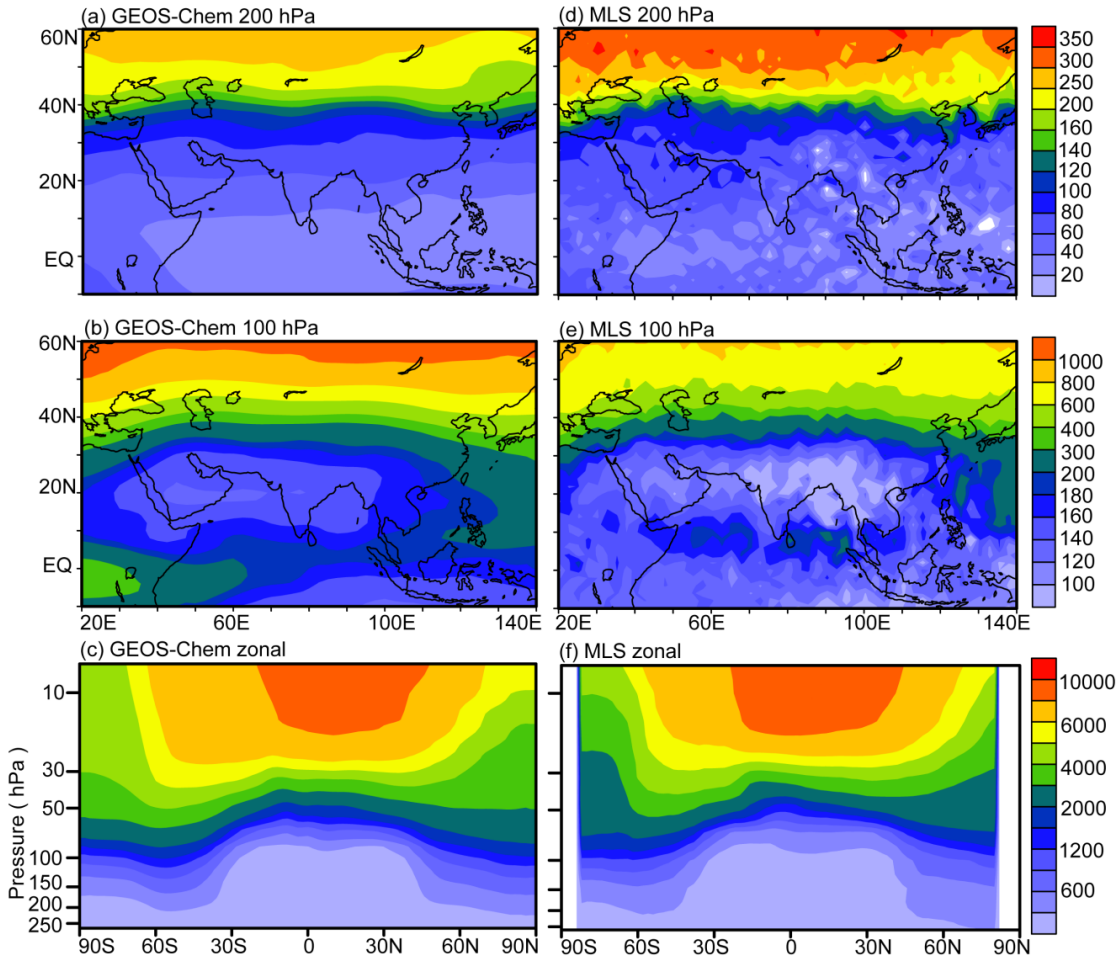

Figure. 5. Comparisons of simulated O_3 concentrations (ppbv) with observations (ppbv) from MLS. (a) and (b) are simulated concentrations at 200 hPa and 100 hPa, respectively. (c) is the latitude-altitude cross section of simulated O_3 concentrations averaged over 70–105°E. (d)-(f) are the same as (a)-(c), except that (d)-(f) are observations from MLS. All the datasets are averaged over June-August of 2005.

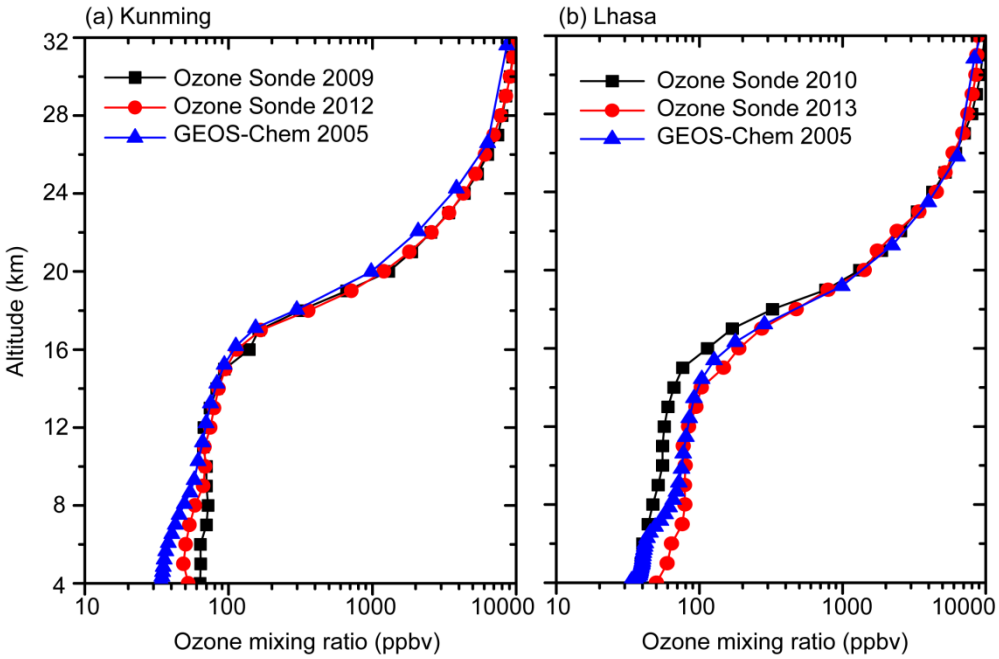

Figure 6. The simulated and observed vertical profiles of monthly mean O_3 mixing ratios at (a) Kunming and (b) Lhasa in August. The model results are from the simulation of year 2005. The observations in Kunming were conducted during August 7–13 (11 profiles of O_3 collected) in 2009 and during August 12–31 in 2012 (daily observations). The observations in Lhasa were conducted during August 22–28 in 2010 (12 profiles of O_3 collected) and during August 4–26 in 2013 (daily observations).

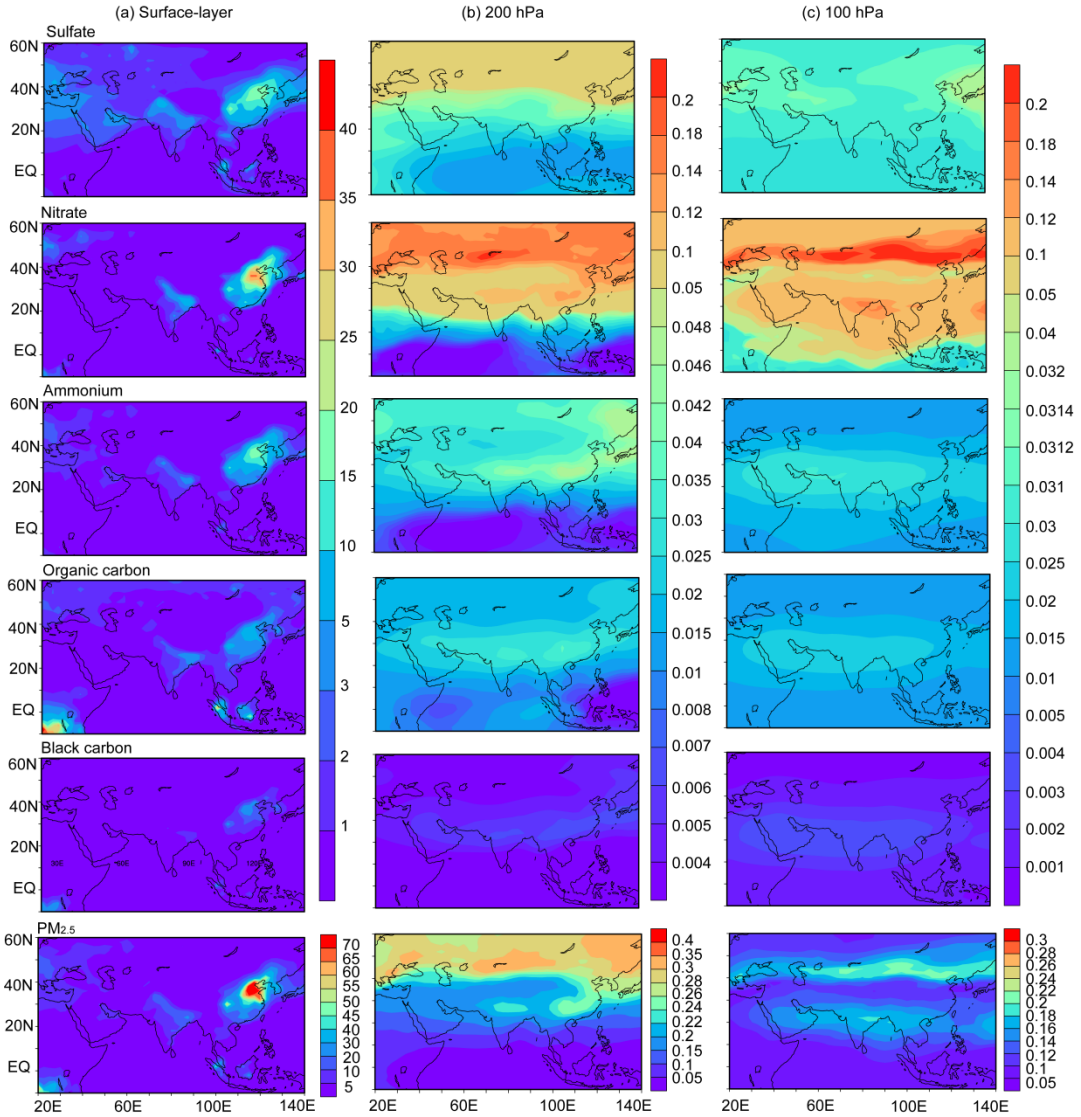

Figure. 7. Simulated seasonal mean concentrations (μg m^{-3}) of sulfate, nitrate, ammonium, organic carbon, black carbon, and $PM_{2.5}$ at (a) the surface layer, (b) 200 hPa, and (c) 100 hPa, during summer (June-August) of year 2005. Note that color bars are different for concentrations at the surface, 200 hPa, and 100 hPa.

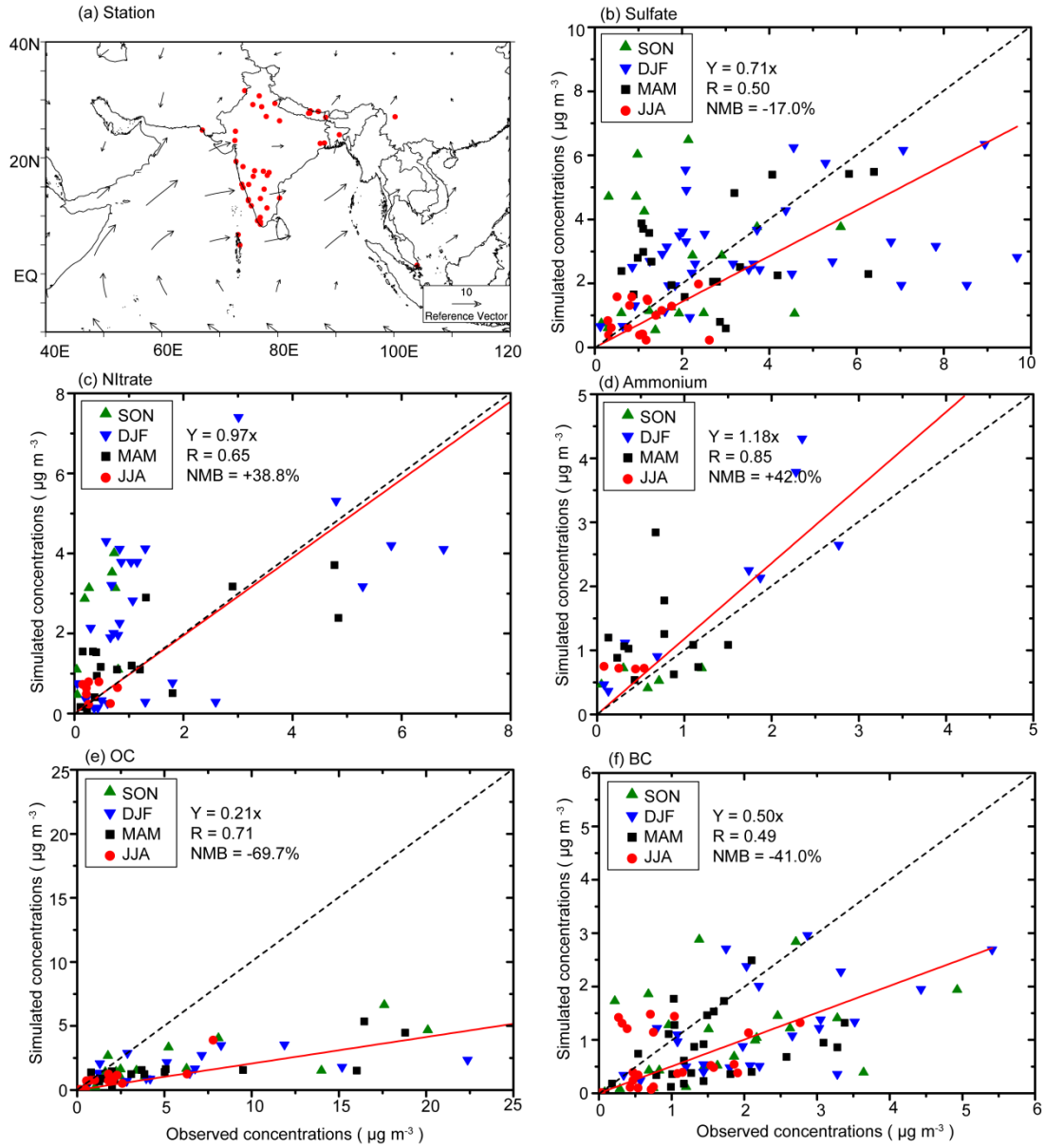

Figure. 8. (a) Locations with measured aerosol concentrations from previous studies. Also shown are surface winds during summertime. (b)–(f) show the comparisons of simulated seasonal mean concentrations of sulfate, nitrate, ammonium, OC, and BC with measured values, respectively. Also shown in (b)–(f) are the 1:1 line (dashed), linear fit (solid line and equation), correlation coefficient between simulated and measured concentrations (R), and normalized mean bias (NMB) (defined as NMB=$\frac{\sum_{i=1}^{n}(P_i-O_i)}{\sum_{i=1}^{n}O_i}$ ×100%, where P_i and O_i are predicted and observed concentrations at station *i* for each aerosol species).

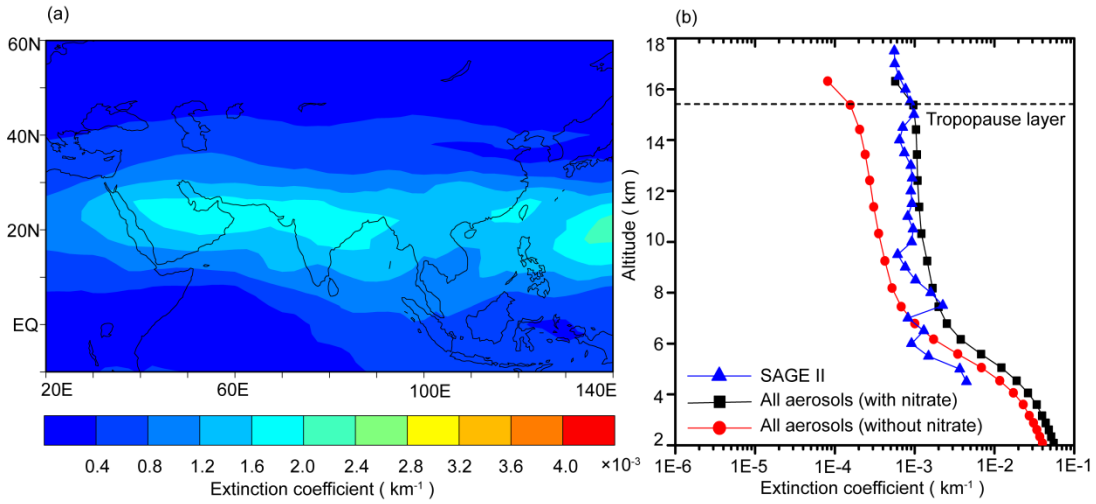

Figure. 9. (a) Monthly mean distribution of aerosol extinction coefficients (km^{-1}) at 100 hPa for July of 2005. (b) Monthly mean vertical distributions of aerosol extinction coefficients (at 525 nm for SAGE II and 550 nm for GEOS-Chem) (km^{-1}) averaged over the Asian monsoon anticyclone region (20–120°E, 10–40°N) for July of 2005. The horizontal dashed line represents the tropopause averaged over the Asian monsoon anticyclone region simulated by the GEOS-Chem model.

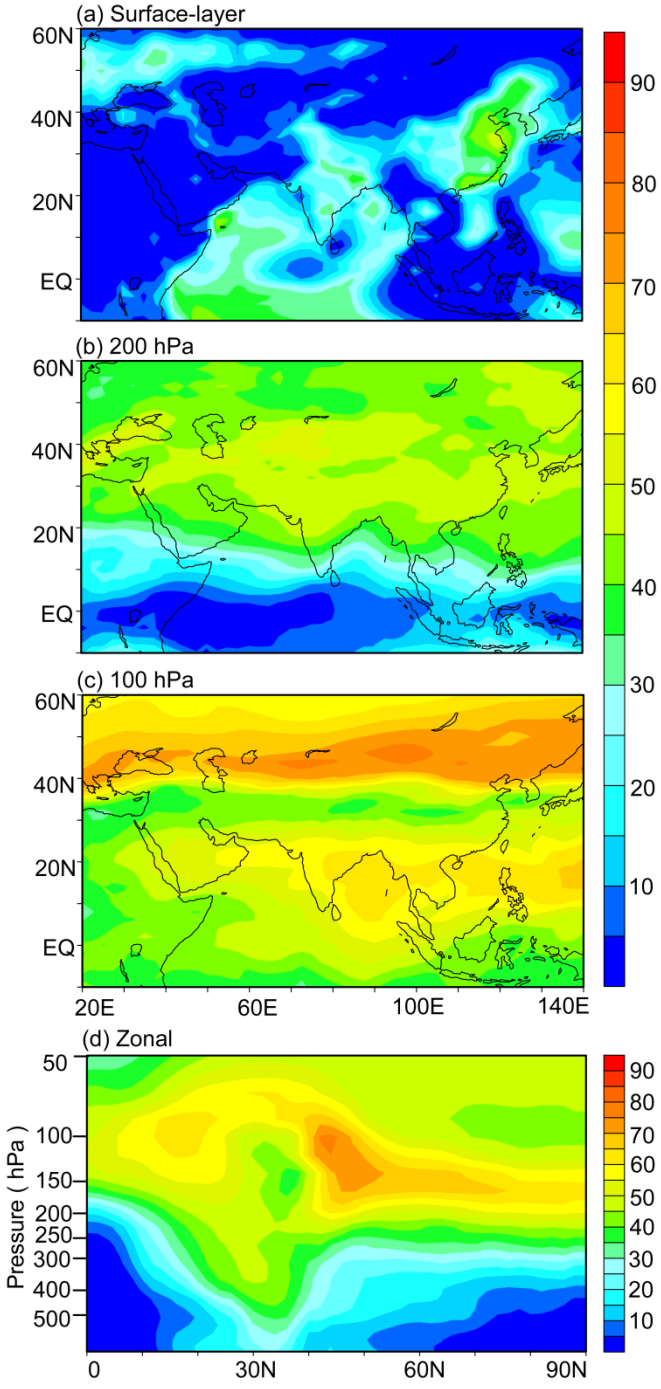

Figure. 10. Simulated contributions of nitrate to $PM_{2.5}$ (C_{NIT}= [NIT]/ [$PM_{2.5}$] ×100%) averaged over summer (June-August) of year 2005 at (a) surface-layer, (b) 200 hPa, and (c) 100 hPa. (d) The latitude-altitude cross section of simulated C_{NIT} (%) averaged over 70–105°E.

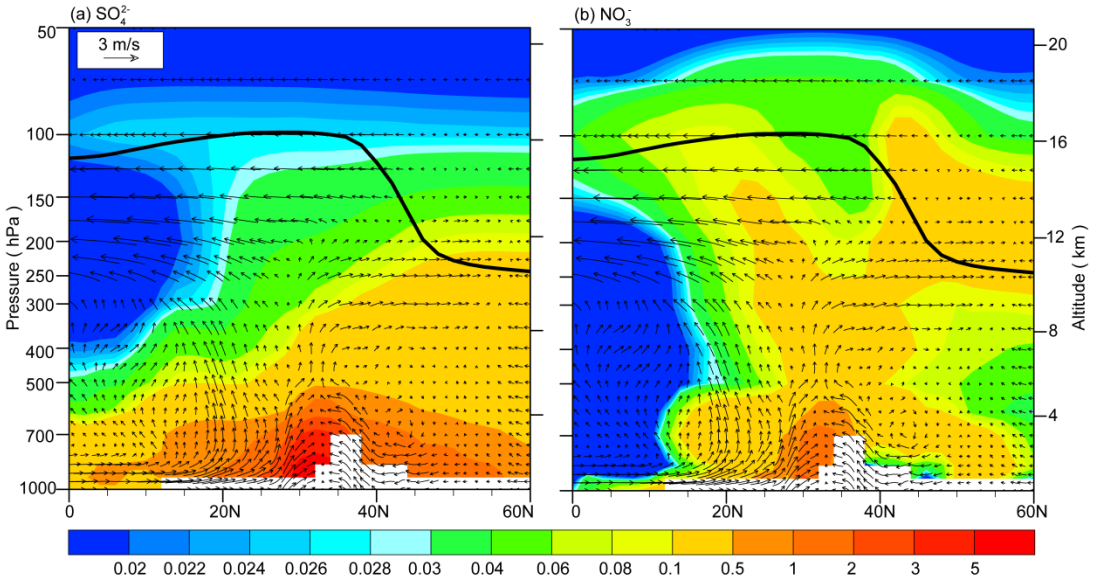

Figure. 11. Latitude-altitude cross sections of simulated concentrations (color shades, μg m^{-3}) of SO_4^{2-} and NO_3^- averaged over 70–105°E in June-August of 2005, together with the wind vectors obtained from the European Centre for Medium-Range Weather Forecasts (ECMWF) ERA-Interim Reanalysis data. The black line is the tropopause simulated by the GEOS-Chem model.

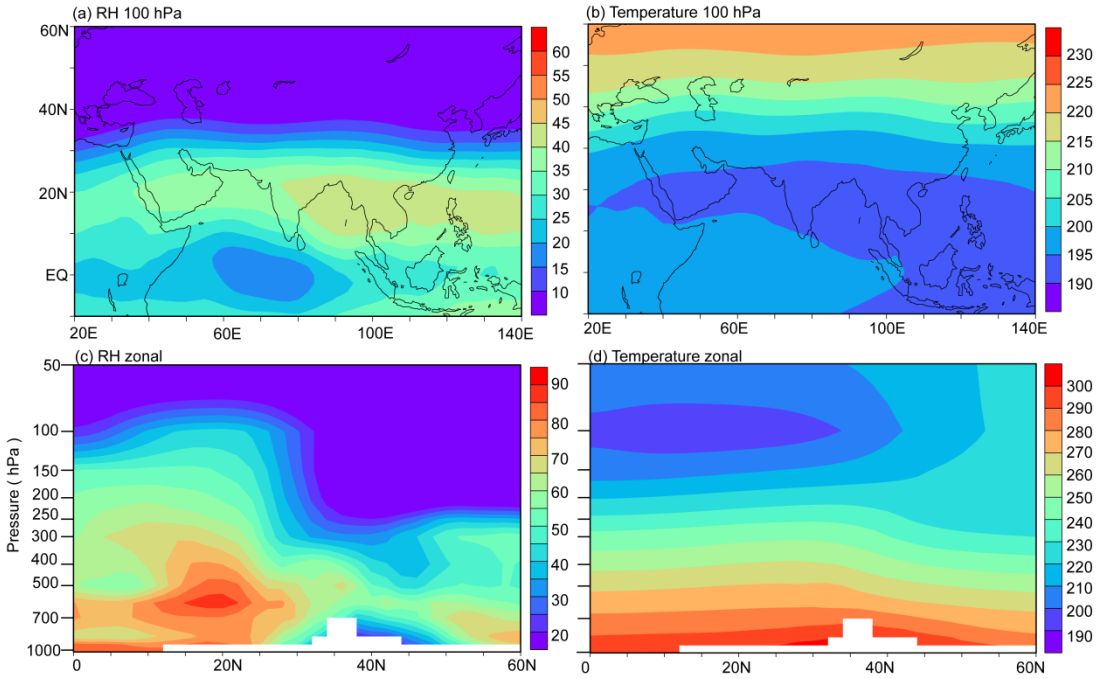

Figure. 12. (a)-(b) Distributions of RH (%) and temperature (K) at 100 hPa. (c)-(d) The latitude-altitude cross sections of RH (%) and temperature (K) averaged over 70–105°E. RH and temperature are from the GEOS5 assimilated meteorological fields, and all the values are the averages over June-August of year 2005.

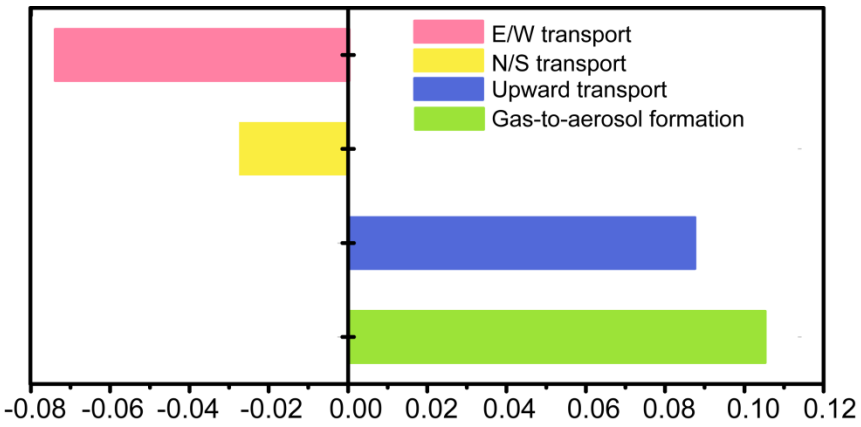

Figure. 13. Mass budget for nitrate aerosol within the selected box of (70–105°E, 10–40°N, 8–16 km). E/W transport indicates net mass flux through the east and west lateral boundaries, N/S transport indicates net mass flux through the north and south lateral boundaries, and upward transport is the net mass flux through the top and bottom sides of the box. The mass flux is positive if it increases nitrate mass within the box. Unit of fluxes is Tg season^{-1}. All the values are the averages over June-August of 2005.